A simple model for assessing climate control trade-offs and responding to unanticipated climate outcomes

Henri F. Drake*[1,2], Ronald L. Rivest[1], Alan Edelman[1], and John Deutch[1]

[1] *Massachusetts Institute of Technology, Cambridge, MA, USA*

[2] *MIT-WHOI Joint Program in Oceanography/Applied Ocean Science & Engineering, Cambridge and Woods Hole, MA, USA*

Abstract

Persistent greenhouse gas (GHG) emissions threaten global climate goals and have prompted consideration of climate controls supplementary to emissions mitigation. We present MARGO, an idealized model of optimally-controlled climate change, which is complementary to both simpler conceptual models and more complicated Integrated Assessment Models. The four methods of controlling climate damage– mitigation, carbon dioxide removal, adaptation, and solar radiation modification– are not interchangeable, as they enter at different stages of the causal chain that connects GHG emissions to climate damages. Early and aggressive mitigation is necessary to stabilize GHG concentrations at a tolerable level. While the most cost-effective way of keeping climate suffering below present-day levels is a combination of all four controls, trade-offs between the different controls are sensitive to value-driven parameters and poorly-known damage costs.

Static policy optimization assumes perfect foresight and obscures the active role decision-makers can have in shaping a climate trajectory. We propose an explicit policy response process wherein climate control targets are re-adjusted over time in response to unanticipated outcomes, and illustrate this process in two "storyline" scenarios: 1) near-term increases in mitigation and carbon dioxide removal are deficient, such that climate goals are expected to slip out of reach; 2) solar radiation modification is abruptly terminated after 40 years of successful deployment, causing an extremely rapid warming which is amplified by an excess of GHGs due to deterred mitigation. In both cases, an optimized policy response yields substantial benefits relative to continuing the original policy.

The MARGO model is intentionally designed to be as simple, transparent, customizable, and accessible as possible, addressing several concerns about previous climate-economic modelling approaches and enabling a more diverse set of stakeholders to engage with these timely and controversial topics.

1 Introduction

Climate change due to anthropogenic greenhouse gas (GHG) emissions poses an existential threat to society (Steffen et al., 2018). Ever since the direct link between GHGs and global warming was established in climate models over fifty years ago (Manabe and Wetherald, 1967), scientists have advocated substantial emissions mitigation to

stabilize global GHG concentrations and temperatures (Revelle et al., 1965). The discovery that humans were unintentionally modifying the climate was unsurprisingly followed by speculation about intentional climate control (Kellogg and Schneider, 1974). With GHG emissions continuing to increase and climate goals slipping out of reach (Peters et al., 2020), the call for serious consideration of climate controls beyond just mitigation grows louder (Buck, 2012; Council et al., 1991; Crutzen, 2006; Parson, 2017; Victor et al., 2009).

Four climate controls have emerged as candidates for use in the future: emissions **M**itigation, carbon dioxide **R**emoval (CDR), **G**eo-engineering by Solar Radiation Modification (SRM), and **A**daptation. The four controls are not directly interchangeable as they enter at different stages of the causal chain of climate damages (Figure 1; Caldeira et al., 2013; Deutch, 2019; Moreno-Cruz et al., 2018):

$$\text{Emissions} \xrightarrow{\mathbf{M}} \text{GHGs} \xrightarrow{\mathbf{R}} \text{Forcing} \xrightarrow{\mathbf{G}} \text{Warming} \xrightarrow{\mathbf{A}} \text{Damages}. \tag{1}$$

Controls further down the causal chain generally carry greater risks, since they require off-setting the downstream effects of GHG emissions, but also have unique advantages: CDR is the only control that decreases GHG concentrations; SRM is quick to deploy, yields immediate results, and has low direct costs (McClellan et al., 2012); and adaptation allows for flexibility in the other controls as any residual climate damages can be reduced by adapting to the new climate, to some extent (Dow et al., 2013).

Numerous social or geopolitical factors may substantially limit or block deployments of certain controls, with solar radiation modification standing out as particularly contentious (Caldeira and Ricke, 2013; Parson and Keith, 2013; Schäfer et al., 2013; Talati and Higgins, 2019). Problems related to inequity (Flegal and Gupta, 2018), distrust (Haerlin and Parr, 1999; Lacey et al., 2018), or lack of governance (Flegal et al., 2019; Ricke et al., 2013) are just a handful of examples. While we do not explicitly include these complexities, we explore them implicitly within parameter sensitivity experiments and in two "storyline" scenarios (Section 4), as recommended by Shepherd et al. (2018). In these scenarios, we explore both: 1) the best (or "optimized") case in which a unitary decision-maker, as a surrogate for the more complicated realistic international policy-making process, prescribes control trajectories and their prescriptions are exactly realized, and 2) more realistic cases (hereafter referred to as "suboptimal") in which control deployments fall short of the prescribed optimal trajectory and the decision-maker thus benefits from readjusting their policies.

Our hypothetical decision-maker must follow some set of principles on which to base their control policies. We explore two commonly-studied approaches: 1) the cost-benefit approach, in which control costs are balanced against the benefits of avoided damages, and 2) the cost-effectiveness approach, in which control costs are minimized subject to a prescribed climate constraint. The cost-effectiveness approach implicitly underlies the Paris Climate Agreement (United Nations Framework Convention on Climate Change, 2015), which currently organizes global climate policy and aims to keep global warming well below 2 °C relative to preindustrial levels.

The conventional tool for optimizing global climate control is the Integrated Assessment Model (IAM), the result of coupling a climate system model to an energy-economy model (see Weyant, 2017, for a general overview of IAMs and their utility to date). In this paper, we 1) present a novel idealized climate-economic model of optimally-controlled climate change and 2) propose a sequential policy process for periodic policy re-evaluation, which we

illustrate by two "storyline" scenarios: A) near-term mitigation and carbon dioxide removal shortfalls (e.g. Peters et al., 2017; Rogelj et al., 2016; United Nations Environment Programme, 2018) and B) abrupt termination of solar radiation modification (e.g. Goes et al., 2011; Matthews and Caldeira, 2007).

2 MARGO: An idealized model of optimally-controlled climate change

The **MARGO** model consists of a physical energy balance model of Earth's climate coupled to an idealized socio-economic model of climate damages and controls (Figure 1):

Mitigation of greenhouse gas emissions,
Adaptation to climate impacts,
Removal of carbon dioxide (CDR),
Geoengineering by solar radiation modification (SRM), and
Optimal deployment of available controls.

Each of the climate controls acts, in its own distinct way, to reduce the damages caused by a changing climate, but also carry their own deployment costs. The model is designed to include key features of climate physics, economics, and policy as concisely as possible. The shortcoming of the model's simplicity is that its quantitative results can not be relied on to quantitatively inform policy decisions, but instead provides intuition about system dynamics and linkages between variables and parameter values.

The model is developed openly using the Julia programming language (Bezanson et al., 2017) at `github.com/ClimateMARGO/ClimateMARGO.jl` and includes comprehensive documentation. The model originated as an extension of a previous analytical model (Deutch, 2019) to time-dependent control variables. Each model component is expressed in closed form to facilitate analytical analysis and computation, such that an entire MARGO optimization problem can be explicitly written down in one or two expressions, for cost-benefit and cost-effectiveness analyses, respectively (see Section S3.1). The parameter values used throughout the paper are set to the defaults mentioned in this section (and comprehensively listed in Table S1), except when exploring parameter sensitivities. Although we tune many of the model parameters based on existing literature and validated the model's behavior against another model (see Sections S1, S5), we caution that our "optimized" results are not reliable for real-world policy recommendations because of the model's simplicity. In a few cases, where the choice of a parameter value is value-dependent or arbitrary, we perform sensitivity explorations to show how our results depend on these choices.

2.1 No-policy baseline scenario

Climate-controlled scenarios are considered relative to an exogenous no-policy baseline where carbon-dioxide equivalent (CO_{2e}) emissions $q(t)$ increase linearly four-fold by 2100 and decrease linearly to zero by 2150 (for reasons independent of climate policy), resulting in $7.3\,\mathrm{W/m^2}$ of radiative forcing by 2100 and $8.5\,\mathrm{W/m^2}$ by 2150, relative to preindustrial levels. As a result of this forcing, global-mean warming reaches $2\,^\circ\mathrm{C}$ by 2050 and soars to $T \approx 4.75\,^\circ\mathrm{C}$ by 2100, relative to preindustrial. We interpret this emission scenario as an idealized extension of the SSP3 baseline scenario, which is characterized by fossil-fueled growth (Riahi et al., 2017).

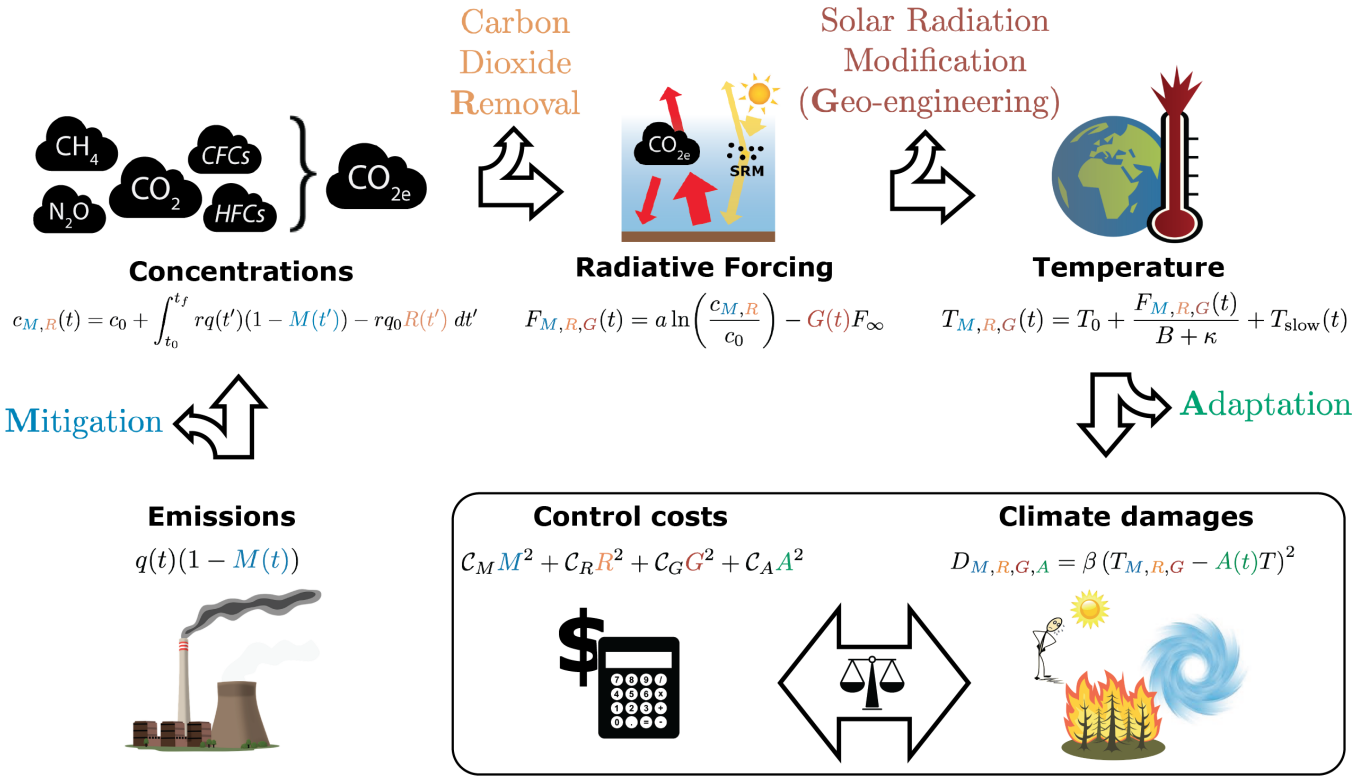

Figure 1: Schematic of the causal chain from greenhouse gas emissions to climate damages, including the unique effects of four climate controls: emissions **M**itigation, carbon dioxide **R**emoval (CDR), **G**eoengineering by Solar Radiation Management (SRM), and **A**daptation. Climate controls yield benefits in terms of avoided climate damages, which are balanced against control deployment costs.

There are five steps in the causal chain (eq. 1 and Figure 1) between CO_{2e} emissions and climate damages:

1. CO_{2e} is emitted at a rate $q(t)$, with only a fraction $r = 50\%$ (Solomon et al., 2009) remaining in the atmosphere after a few years, net of uptake by the ocean and terrestrial biosphere[1].
2. CO_{2e} concentrations accumulate as long as the emissions $q(t)$ are non-zero.
3. Increasing CO_{2e} concentrations strengthen the greenhouse effect, reducing outgoing longwave radiation and causing an increased radiative forcing $F(t)$, which exerts a warming effect on the surface.
4. Near-surface air temperatures increase by $\Delta T = T(t) - T(t_0)$ to balance the reduced cooling to space.
5. Anthropogenic warming causes a myriad of climate impacts, which result in economic damages $D(t) = \beta T^2$.

2.2 Effects of climate controls

The four available climate controls enter as fractional controls at each link of the climate change causal chain (eq. 1). Each control is parameterized such that its full deployment would, in isolation, roughly remove or offset the climate damages due to the baseline emissions. This normalization allows a meaningful quantitative comparison of the control deployment variables.

Mitigation reduces emissions by a factor $M(t) \in [0, 100\%]$ such that controlled emissions are given by $q(t)\,(1-M(t))$, where $M = 100\%$ corresponds to complete decarbonization of the economy.

Removal of CO_{2e}, $R(t) \in [0, 100\%]$, is de-coupled from instantaneous emissions and is expressed as the fraction of 2020 baseline emissions that are removed from the atmosphere in a given year, $q_0 R(t)$. A maximal value of $R = 100\%$ thus corresponds to removing $59\,\mathrm{GtCO_{2e}}$/year, which is more than twice a recent upper-bound estimate of $24.5\,\mathrm{GtCO_{2e}}$/year for "feasible" potential deployments of negative emission technologies (Fuss et al., 2018).

A useful diagnostic quantity is the effective emissions

$$r[q(t)(1 - M(t)) - q_0 R(t)], \tag{2}$$

which is the annual rate of CO_{2e} accumulation in the atmosphere (Figure 2a). The change in CO_{2e} concentrations is the integral of the effective emissions over time (Figure 2b),

$$c_{M,R}(t) = c_0 + \int_{t_0}^{t} rq(t')(1 - M(t')) - rq_0 R(t')\ \mathrm{d}t'. \tag{3}$$

Geoengineering by SRM, $G(t) \in [0, 100\%]$, acts to offset a fraction of the CO_{2e} forcing (Figure 2c),

$$F_{M,R,G}(t) = F_{M,R}(t) - G(t)F_\infty, \tag{4}$$

where $F_{M,R} = a \ln(c_{M,R}(t)/c_0)$ is an empirically-determined CO_{2e} forcing function (with $a = 5\,\mathrm{W/m^2}$) and $F_\infty = 8.5\,\mathrm{W/m^2}$ is the maximum baseline CO_{2e} forcing, which is attained starting in 2150 when baseline emissions are assumed to reach zero. A value of $G = 100\%$ thus corresponds to a complete cancellation between the equilibrium

[1]The model's realism would be improved replacing this crude carbon accounting model with a non-linear model of the ocean carbon cycle (e.g. Glotter et al., 2014), but this would considerably complicate the exposition and interpretability of MARGO's equations.

warming from baseline CO_{2e} increases and the cooling from a full deployment of SRM. Since the model timestep $\delta t = 5$ years is longer than the 1 year residence timescale of aerosols in the stratosphere (the most likely and persistent SRM technology candidate; Robock et al. 2008), its effects are instantaneous and have no memory: the cooling effect of SRM ends as soon as its deployment ends. Inefficiencies (Visioni et al., 2017) or inefficacies (Modak et al., 2016) in the SRM forcing mechanism do not appear explicitly and instead are factored into the SRMs deployment costs below.

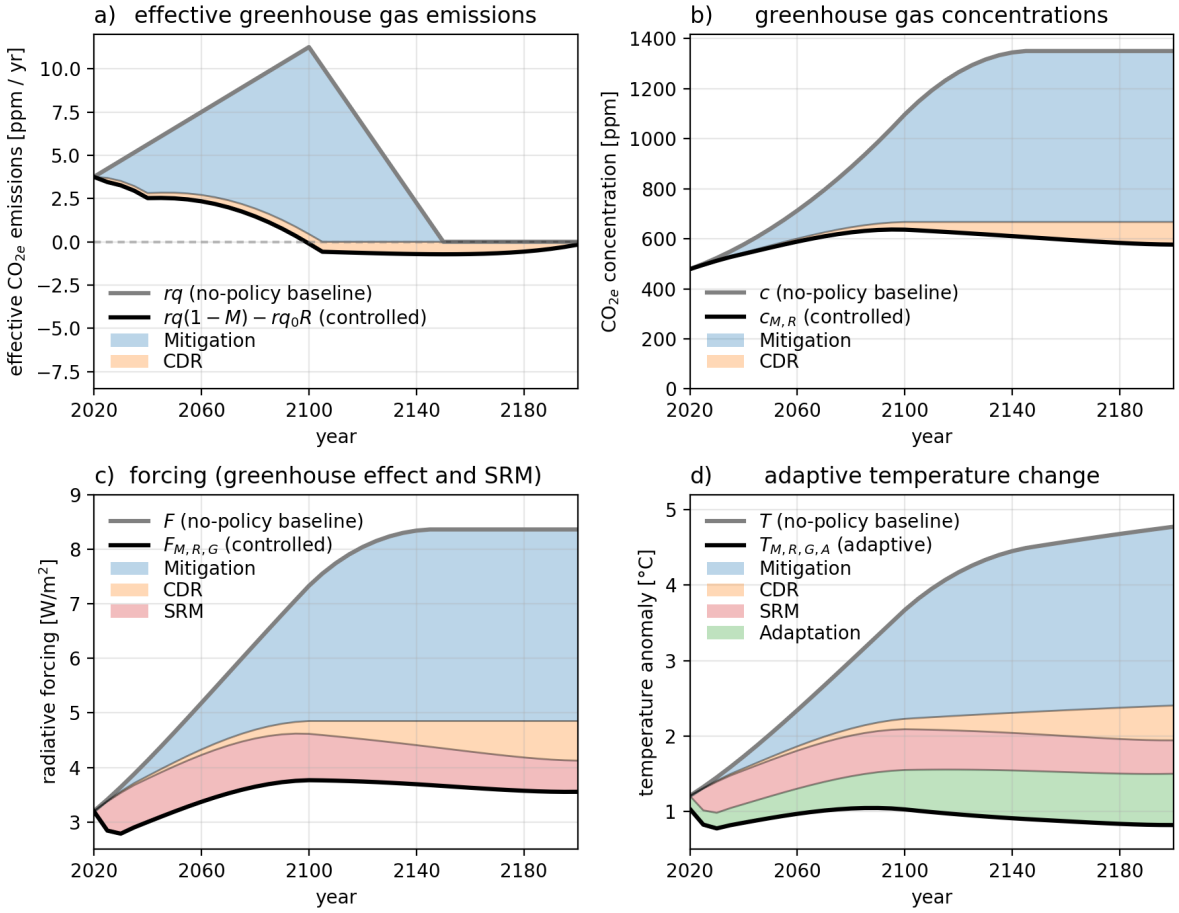

Figure 2: Baseline (thick grey line) and optimally cost-beneficial (thick black line) a) effective CO_{2e} emissions, b) CO_{2e} concentrations, c) radiative forcing, and d) temperature change (relative to preindustrial). Colored wedges show a natural decomposition of the effects of the four different climate controls, computed by setting downstream controls to zero in (5): **M**itigation (blue); carbon dioxide **R**emoval (CDR; orange); solar radiation modification (SRM) or **G**eoengineering (red); and **A**daptation (green). Adaptation does not directly affect realized temperatures but is included in the plot using the adaptive pseudo-temperature construct (eq. 7). Equivalent curves for the cost-effectiveness analysis are shown in Figure S8.

The controlled warming (Figure 2d), given by the deep-layer energy balance model solution

$$T_{M,R,G}(t) - T_0 = \frac{F_{M,R,G}(t)}{B+\kappa} + \frac{\kappa}{B}\int_{t_0}^{t} \frac{e^{\frac{t'-t}{\tau_D}}}{\tau_D} \frac{F_{M,R,G}(t')}{B+\kappa}\,\mathrm{d}t', \tag{5}$$

evolves in response to the total controlled forcing $F_{M,R,G}$, where $T_0 = 1.1\,^\circ\mathrm{C}$ is the present warming relative to preindustrial, $B = 1.13\,\mathrm{W/m^2/K}$ is the climate feedback parameter, $\kappa = 0.73\,\mathrm{W/m^2/K}$ is the ocean heat

uptake rate, and $\tau_D = 240$ years is a slow deep ocean timescale (Geoffroy et al., 2012). If forcing is stabilized for sufficiently long ($\Delta t \gg \tau_D$), warming asymptotes to an equilibrium response $T_{M,R,G} - T_0 = F_{M,R,G}/B$. Transiently, $B/(\kappa + B) = 60\%$ of the warming occurs effectively instantaneously (first term on right-hand side of eq. 5), while the remaining $\kappa/(B + \kappa) = 40\%$ is spread out over centuries due to the thermal inertia of the deep ocean (second term). This climate inertia decouples the temperature response from instantaneous forcing and implies that some warming (or cooling) is locked in for the future, even if radiative forcing is stabilized (Lickley et al., 2019), as in the case of bringing emissions to zero in our model[2]. We derive, interpret, and validate this energy balance model solution in greater detail in Section S1.

Adaptation to climate impacts acts to reduce damages by a fraction $A(t)$ of the baseline damages. Controlled damages are thus given by

$$D_{M,R,G,A} = \beta \left(T_{M,R,G} - A(t)T\right)^2, \tag{6}$$

where the damage parameter β is tuned such that warming of 3 °C results in damages of the 2% of Gross World Product (GWP) in the absence of adaptation, consistent with DICE's damage function in the limit of non-catastrophic warming (Nordhaus and Sztorc, 2013). Since some climate impacts are likely impossible to adapt to (Dow et al., 2013), we arbitrarily assume that adaptation can at most reduce climate damages by 40% of the baseline (i.e. $A \in [0, 40\%]$). However, available estimates of adaptation costs are relatively high, such that preferences for adaptation are sufficiently low that this upper bound is never reached in our results. Although adaptation does not affect the planetary temperature directly, it is useful to consider an "adaptive" pseudo-temperature $T_{M,R,G,A}$ (Figure 2d) which yields controlled damages equivalent to the fully-controlled damages $\beta(T_{M,R,G,A})^2 = \beta(T_{M,R,G} - A(t)T)^2$ and is defined

$$T_{M,R,G,A} \equiv T_{M,R,G} - A(t)T. \tag{7}$$

2.3 Costs and benefits of controlling the climate

The costs of deploying climate controls are non-negligible and must be balanced against the benefits of controlling the climate to avoid climate impact damages. The costs of climate controls are parameterized as:

$$\mathcal{C} = \mathcal{C}_M M^2 + \mathcal{C}_R R^2 + \mathcal{C}_G G^2 + \mathcal{C}_A A^2, \tag{8}$$

where $C_M = 34$ USD per tCO_{2e} (marginal cost of 68 USD per tCO_{2e} at $M = 100\%$), $\mathcal{C}_R = 440$ USD per tCO_{2e}, $\mathcal{C}_G = 12.6\,\%$ of GWP per 8.5 W/m^2 of SRM (equal to the climate damages from the same amount of CO_{2e} forcing), and $\mathcal{C}_A = 18$ trillion USD per year are the hypothetical annual costs of full deployment used in the default scenario (details in Section S2, loosely based on Clarke et al. 2014; Fuss et al. 2018; Global Commission on Adaptation 2019). These cost functions are convex functions of fractional deployment with zero initial marginal cost, (as in Moreno-Cruz et al., 2018; Nordhaus, 1992), and are here all taken to be quadratic for simplicity, such that marginal control costs increase linearly with the deployment fraction. The benefits of deploying climate controls are the

[2]In earth system models with a dynamic carbon cycle, the slow recalcitrant warming due to a reduction in ocean heat uptake happens to be roughly offset by the ocean carbon sink (Solomon et al., 2009), such that bringing emissions to zero roughly stabilizes temperatures (Matthews and Caldeira, 2008).

avoided climate damages relative to the no-policy baseline scenario,

$$\mathcal{B} = D - D_{M,R,G,A} = \beta(T^2 - (T_{M,R,G,A})^2). \tag{9}$$

2.4 Exogenous economic growth

We treat economic growth as exogenous: it is represented by the GWP $E(t) = E_0(1+\gamma)^{(t-t_0)}$, and grows from its present value of $E_0 = 100$ trillion USD with a fixed growth rate $\gamma = 2\%$, consistent with expert opinion and an econometric forecast model (Christensen et al., 2018). We ignore feedbacks of climate abatement costs and climate damages on economic growth, since they are small variations relative to the exponential rate of economic growth in many IAM implementations[3] (Azar and Schneider, 2002; Nordhaus and Sztorc, 2013).

3 Optimizing a balanced climate policy portfolio

The surrogate climate policy decision-maker specifies an objective function to maximize, subject to additional policy constraints, and MARGO is readily optimized in terms of its time-dependent climate controls. The optimization is implemented in Julia using the Interior Point Optimizer (Wächter and Biegler, 2006) and runs in a fraction of a second (Figure S4); see details in Section S4.1 (some additional policy constraints required by the optimization problem, such as maximum deployments and maximum deployment rates, are described in Section S3.2). Here, we describe the optimally-controlled results of two policy approaches, cost-benefit analysis and cost-effectiveness analysis, and explore their sensitivity to key value-driven or poorly-known parameters. See Figures S6 and S7 for intuitive visualizations of the one– and two–dimensional versions of the optimization, respectively.

3.1 Cost-benefit analysis

A natural and widely-used approach is cost-benefit analysis, in which the cost $\mathcal{C}_{M,R,G,A}$ of deploying climate controls is balanced against the benefits $\mathcal{B}_{M,R,G,A}$ of avoiding climate damage. Formally, we aim to maximize the net present benefits[4]:

$$\max\left\{\int_{t_0}^{t_f} \left(\mathcal{B}_{M,R,G,A} - \mathcal{C}_{M,R,G,A}\right)(1+\rho)^{-(t-t_0)}\,\mathrm{d}t\right\}, \tag{10}$$

where ρ is a social discount rate that determines the annual depreciation of future costs and benefits of climate control to society. There are different views about the appropriate discount rate to apply to multi-generational social utility (Arrow et al., 2013; Ramsey, 1928; Solow, 1974; Stern et al., 2007). Here, we choose a default discount rate of $\rho = \gamma = 2\%$ (zero pure time discount rate), which is on the low end of values used in the literature due to our preference towards inter-generational equity (Schneider, 1989).

[3]However, recasting the negative feedback of temperature on economic growth in terms of climate damages increases the damage function and leads to more stringent optimized mitigation policies (Glanemann et al., 2020; Moore and Diaz, 2015).

[4]This is equivalent to the conventional formulation of maximizing welfare changes $\Delta W = \int \lambda \Delta C\,\mathrm{d}t$, where $\Delta C = \mathcal{B} - \mathcal{C}$ is a change in consumption, $\lambda(t)$ is a discount factor. We assume a logarithmic utility function such that consumption changes are effectively discounted at a rate $-\dot{\lambda}/\lambda = \dot{C}/C + \delta \approx \gamma + \delta$, where δ is the pure time discount rate (Stern et al., 2007) and we assume similar growth rates for production and consumption $\dot{C}/C \approx \gamma$ (Kelleher and Wagner, 2019). We define $\rho \equiv \gamma + \delta$ to be the discount rate that describes exponential discounting $\lambda(t) \propto e^{-\rho t}$, which by expansion for $\rho \ll 1$ gives us the form $\lambda(t) \propto (1-\rho t) \propto (1+\rho)^{-t}$ used here.

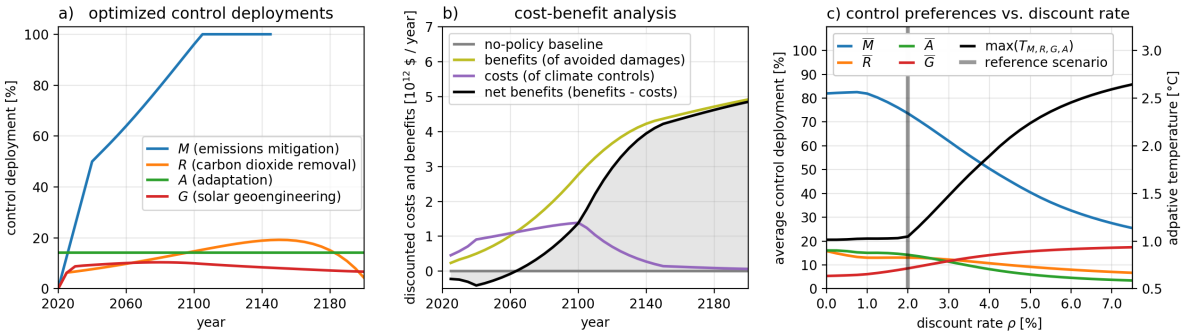

Figure 3: Results of cost-benefit analysis and their sensitivity to the discount rate ρ. (a) Optimized fractional control deployments and (b) corresponding discounted costs and benefits relative to the no-climate-policy baseline scenario. The mitigation curve in (a) ends in 2150 because baseline emissions go to zero and there is nothing to mitigate thereafter. The total positive area shaded in grey in (b) is the maximum net present benefit (eq. 10), defined as the benefits (green) minus the costs (purple). Since the discount rate is equal to the economic growth rate and $E_0 = 100 \times 10^{12}$ USD/year, the y-axis in (b) can also be read as a percentage of GWP in a given year. (c) Time-mean control deployments (left axis) and maximum adaptive temperatures (right axis), as a function of the discount rate.

The results of maximizing net present benefits are shown in Figure 3. Early and aggressive emissions mitigation– and to a lesser extent CDR (Fig 3a)– drive net discounted costs of 0.5 trillion USD/year relative to the no-policy baseline but begin delivering orders of magnitude more in net discounted benefits after the break-even point in 2065 (Fig 3b; Brown et al. 2020). Effective CO_{2e} emissions reach net-zero by 2100, such that concentrations stabilize below $c_{M,R} < 700\,\text{ppm}$ and are brought back down below $c_{M,R} = 600\,\text{ppm}$ by 2200 (Figure 2a,b) as CDR is ramped up to $R = 20\%$ (or $q_0 R \approx 6\ \text{GtCO}_{2\text{e}}\,/\,\text{year}$). Moderate SRM deployments of about $G = 10\%$ (cooling of $0.9\,\text{W/m}^2$; Figure 2c) lowers the maximum warming from $T_{M,R} \approx 2.1\,^\circ\text{C}$ to $T_{M,R,G} \approx 1.6\,^\circ\text{C}$ above preindustrial (Figure 2d). Moderate deployments of adaptation offset 16% of baseline climate damages, such that optimized adaptive temperatures remain roughly below present-day values.

The maximum adaptive temperature that results from cost-benefit analysis is sensitive to the choice of the discount rate ρ (Figure 3c): as the discount rate increases above the economic growth rate (Tol, 2003), $\rho > \gamma = 2\%$, the optimized maximum warming increases from $\max(T_{M,R,G,A}) < 1.1\,^\circ\text{C}$ up to $\max(T_{M,R,G,A}) > 2\,^\circ\text{C}$ if $\rho > 4.5\%$. This increase is largely due to a precipitous decline in emissions mitigation, as near-term mitigation costs are traded for heavily discounted future climate suffering. While optimized CDR and adaptation deployments also decrease with the discount rate, they are roughly offset by increasing SRM, which becomes almost as preferable as mitigation at high discount rates which conceal its high future costs.

3.2 Cost-effectiveness of avoiding damage thresholds

The conventional cost-benefit approach to understanding climate change is limited by the poorly-understood damage function (Koomey, 2013), especially at high levels of forcing (Alley et al., 2003; Burke et al., 2015), and sensitive to value judgements about appropriate discounting. An alternative approach, which presently guides global climate policy negotiations, is to prescribe a threshold of climate damages– or temperatures, as in the Paris Climate

Agreement (United Nations Framework Convention on Climate Change, 2015)– which is not to be surpassed.

In MARGO's cost-effectiveness formulation, we aim to find the lowest net present costs of control deployments

$$\min\left\{\int_{t_0}^{t_f} \mathcal{C}_{M,R,G,A}(1+\rho)^{-(t-t_0)}\ \mathrm{d}t\right\} \tag{11}$$

which keep controlled damages below the level corresponding to a chosen adaptive temperature threshold, $\beta(T_{M,R,G,A})^2 < \beta(T^\star)^2$, which we rewrite as

$$T_{M,R,G,A} < T^\star, \tag{12}$$

where $T_{M,R,G,A}$ is the adaptive temperature (7). The benefit of a formulation based on adaptive temperatures is that it allows all four controls to be explicitly included in cost-effectiveness analysis, which typically only consider mitigation and CDR; the drawback is that our parameterizations for the effects of SRM and adaptation on climate damages are not as well justified as those for mitigation and CDR.

Suppose the decision-maker's goal is to stabilize climate damages below present-day levels, i.e. $T_{M,R,G,A} < T^\star = T_0 = 1.1\,^\circ\mathrm{C}$, at the lowest discounted cost. The results of this cost-effectiveness optimization (SI Figures 1 & 2) are qualitatively similar to the cost-benefit analysis above and are summarized as follows: substantial emissions mitigation keep $T_M < 2.3\,^\circ\mathrm{C}$ by 2100; sustained CDR brings warming down to $T_{M,R} = 2.15\,^\circ\mathrm{C}$ by 2200; SRM shaves off another $\Delta T_G = T_{M,R} - T_{M,R,G} = 0.6\,^\circ\mathrm{C}$ of warming at its peak in 2100; and moderate levels of adaptation are used to keep $T_{M,R,G,A} < T_0 = 1.1\,^\circ\mathrm{C}$ at all times.

The relative importance of SRM in this cost-effectiveness optimization is sensitive to its poorly-known cost and the value-dependent discount rate (Figure 4). For the conservative low SRM cost used here, less than 10% of the optimized cooling is achieved with SRM at low discount rates ($\rho < 1\%$), while more than 50% is achieved with SRM at high discount rates ($\rho > 5\%$). Similarly, if SRM costs are reduced by an order of magnitude, more than 50% of the adaptive cooling (relative to the baseline warming) is achieved with SRM even under the low default discount rate $\rho = 2\%$.

4 A policy process for responding to policy shortfalls and climate surprises

The cost-benefit and cost-effectiveness calculations presented above assume the surrogate policy decision-maker has perfect foresight and that their prescribed optimal control policies are perfectly implemented, such that the anticipated climate outcomes are exactly realized. Here, we present a policy process that allows the decision-maker to respond to suboptimal outcomes, such as policy shortfalls or climate surprises.

4.1 The policy response process

Step 1: The process begins with a single optimization, which produces optimized climate control trajectories and corresponding projections of climate outcomes, from an initial vantage point of t_0 (e.g. present-day).

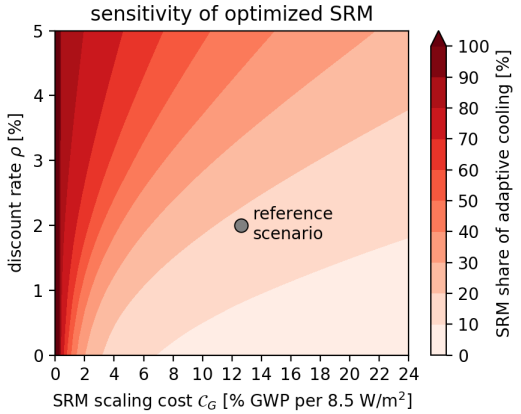

Figure 4: Sensitivity of optimally cost-effective SRM deployments to the discount rate ρ and SRM scaling cost $\mathcal{C}_G$. Colored contours show SRM's average share of the cooling required to keep adaptive warming $T_{M,R,G,A}$ below the threshold $T^\star$, normalized by the baseline temperature deficit $T^\star - T$. A value of 100% corresponds to an SRM-only control portfolio, whereas a value of 0% means only other controls are used. The grey dot shows the location of the relatively conservative (risk-averse) default values used here, where SRM provides roughly 15% of the required cooling.

Step 2: Time advances, $t \to t_1 = t_0 + \Delta t$, such that climate control deployments and outcomes take on their realized values over this period. From the vantage point of the decision-maker in t_0, these outcomes will be suboptimal by definition if they differ from the original optimized projections.

Step 3: To account for policy changes in response to realized climate outcomes, climate control deployments are re-optimized, now from the vantage point of t_1 and with modified policy constraints or parameter values.

Step 4: Repeat, as desired, starting from Step 2, advancing in time to $t_{n+1} = t_n + \Delta t$.

This policy response process is illustrated below via two "storyline" scenarios (Shepherd et al., 2018).

4.2 Storyline A: Mitigation and carbon dioxide removal shortfalls

A surrogate decision-maker prescribes the most cost-effective control trajectories for keeping $T_{M,R} < T^\star = 1.5\,°\text{C}$ (Figure 5a–c, solid black lines), omitting SRM and adaptation, and thus calls for a rapid ramp-up of emissions mitigation ($M = 95\%$ by 2060) and CDR ($R = 40\%$ by 2050). Suppose that, by $t_1 = 2030$, $\Delta t = 10$ years later, it becomes apparent that these anticipated increases in mitigation and CDR have not been met, and realized control deployments instead fall short by $s = 60\%$ (the *shortfall* parameter) between $t_0 = 2020$ and $t_1 = 2030$. If this trend were to continue, and only $1 - s = 40\%$ of mitigation and CDR were to be deployed between 2020 and 2150, then temperatures would skyrocket, eventually reaching 3.8 °C by 2200 (black dashed lines).

Instead, the decision-maker responds by re-optimizing the model, now from the vantage point of $t_1 = 2030$, prescribing a larger ramp-up of CDR to compensate for the previous control shortfalls (Figure 5c). However, short-term mitigation and CDR increases are constrained by the maximum deployment rate (see Section S3.2), such that even the most ambitious deployments allowed by the model result in warming that overshoots the target $T^\star = 1.5\,°\text{C}$ by 0.1 °C (Figure 5a, lowest transparent line). The decision-maker is thus forced to relax their temperature goal,

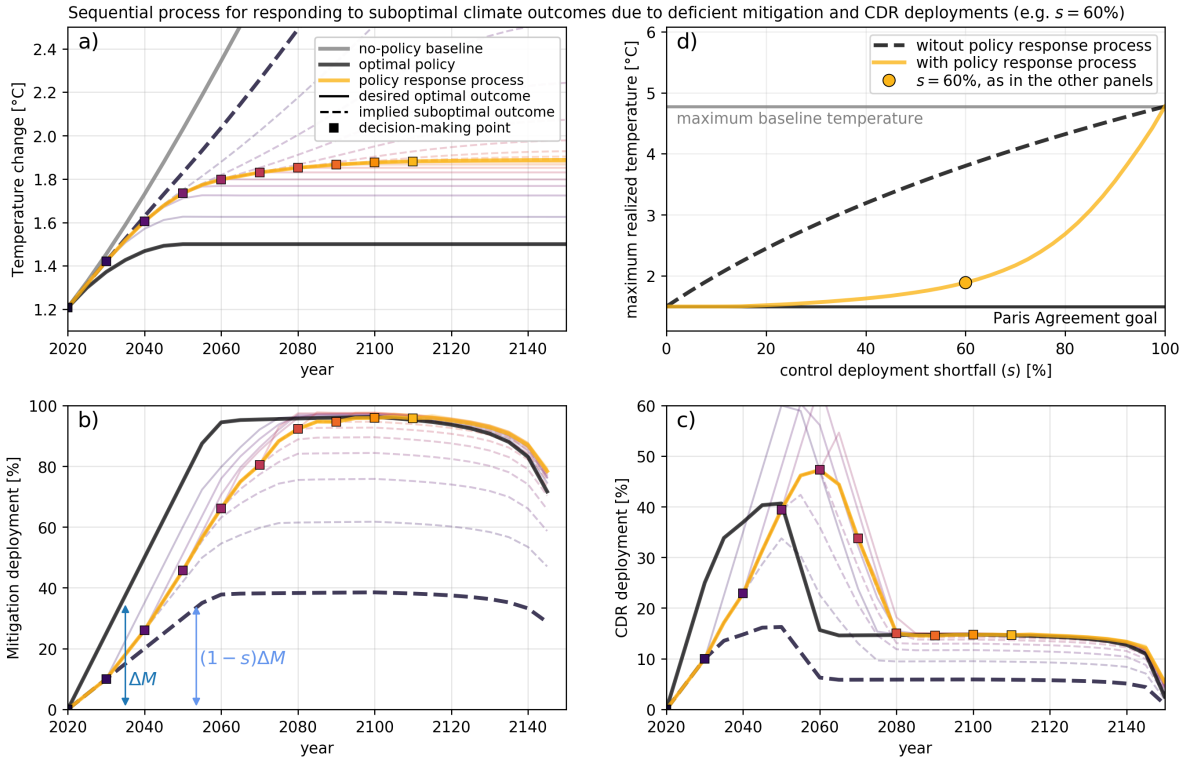

Figure 5: **Storyline A:** a surrogate policy decision-maker prescribes optimized mitigation and carbon dioxide removal (CDR) trajectories which would limit warming below 1.5 °C (thick black lines), but realized deployments repeatedly fall short of these control targets by a fraction s, the *shortfall*. In the absence of a policy response, these control shortfalls lead to a substantial overshoot of the $T^\star = 1.5\,°\mathrm{C}$ goal (thick dashed lines). Panels a)–c) illustrate a policy process for sequentially responding to these control shortfalls every $\Delta t = 10\,\mathrm{years}$, for an arbitrary example value $s = 60\%$. After computing an optimized future projection, $M \to M + \Delta M$ (thin solid lines), realized climate controls are incremented suboptimally, $M \to M + (1-s)\Delta M$ (thin dashed lines; see also annotated arrows). After $\Delta t = 10\,\mathrm{years}$ of realized shortfalls (gold line from one square to the next), the decision-maker re-optimizes their prescription of future deployments, and the process repeats. For $s = 60\%$, a temporary shortfall in mitigation (b) and CDR (c) results in an overshoot of the temperature goal by 0.4 °C (a), although temperatures are eventually stabilized at this level by a delayed decarbonization of $M \approx 100\%$ (b) and intensified CDR deployments (c), which partially compensates for earlier control shortfalls. Panel b) shows how the maximum realized temperature asymptotes to the temperature goal of 1.5 °C for $s < 30\%$ in the optimal limit and to the catastrophic baseline warming of 4.75 °C in the sub-optimal limit of no climate control ($s \to 100\%$).

i.e. increase $T^\star$, if the optimal solution is to satisfy the temperature constraint (details in Section S4.2). Suppose this sequential process repeats every $\Delta t = 10$ years, such that incremental deployments of mitigation and CDR always fall short of the decision-maker's control prescriptions by 60% (thin dashed lines) and the decision-maker responds by prescribing ever more ambitious future control deployments in an attempt to compensate for this previous shortfalls (thin solid lines). As time passes, realized control deployments converge towards their optimal response trajectories, and temperatures eventually stabilize, although they overshoot the original temperature goal $T^\star$ by 0.4 °C (gold lines).

A shortfall of $s = 60\%$ was chosen arbitrarily because it yields moderate but visually distinguishable results (Figure 5a–c). Figure 5b shows the sensitivity of the maximum realized warming as a function of the control deployment shortfall s, which is varied from 0% (optimal) to 100% (zero controls). In the absence of a policy response, the realized warming increases roughly linearly the the shortfall, such that even a small shortfall of 10% results in a 0.5 °C overshoot of the $T^\star = 1.5$ °C goal (Figure 5d, dashed line). The policy response process (gold line), however, yields dramatically better outcomes and allows some room for error. Moderate shortfalls ($s \lesssim 30\%$) yield higher control costs, but the decision-maker still has enough room to compensate for earlier shortfalls and keep warming below the goal of $T^\star = 1.5$ °C. It is only for large shortfalls ($s > 50\%$) that the maximum realized warming increases rapidly with s, reaching 2 °C at $s = 65\%$ and asymptopting to the baseline warming of 4.75 °C in the limit of $s \to 100\%$ (zero control deployments).

Alternatively, the decision-maker may first attempt to only relax the temperature constraint for the short term ($t < 2100$), allowing a temporary overshoot of the temperature goal to buy time for CDR to compensate for excess emissions, before resorting to relaxing the long-term ($t \geq 2100$) temperature constraint if required (Figure S10). While allowing a temporary temperature overshoot allows temperature goals to be met for twice as large a shortfall as the more rigid process above, it requires betting on large CDR deployments ($R = 90\%$ by 2090) which brush the limits of feasibility (Fuss et al., 2014, 2018).

4.3 Storyline B: Abrupt termination of solar radiation modification

In $t_0 = 2020$, a surrogate decision-maker prescribes the most cost-beneficial combination of emissions mitigations, CDR, and SRM (hereafter Yes-SRM; Figure 6). Suppose that after a perfect deployment of these control trajectories for $\Delta t = 40$ years, yielding optimal climate outcomes, the policy decision-maker decides to abruptly cancel SRM deployments (within one model timestep $\delta t = 5$ years) and forbid their future use (Figure 6e; see Parker and Irvine 2018 for a discussion of this storyline's plausibility). The abrupt termination of SRM forcing results in an abrupt warming of 0.6 °C over a decade (Term-SRM; Figure 6), known as a "termination shock". To counteract additional future damages due to this unanticipated warming, the policy decision-maker responds by re-optimizing their portfolio of future climate deployments (Term-Response), from the vantage point of $t_1 = 2060$, prescribing enhancements to mitigation and CDR which accelerate the approach to net-zero emissions by 10 years and cause 0.35 °C less warming by 2200 than in Term-SRM (Figure 6). Despite the increases in controls after $t_1 = 2060$ due to this policy response, CO_{2e} concentrations (Figure 6b) and warming (Figure 6a) remain higher than in a counterfactual world in which SRM was never allowed (No-SRM; Figure 6). This "moral hazard" (Lin, 2013;

McLaren, 2016), whereby investment in SRM deters emissions mitigation and CDR, amplifies the termination shock by an additional 0.05 °C and results in a persistent increase in CO_{2e} levels of 50 ppm relative to No-SRM. A rapid warming of 0.5 °C would likely result in substantial damages and pose challenges to adaptation. However, the termination shock considered here, which occurs within a balanced control portfolio including substantial mitigation and CDR, is only a fraction of the >1 °C/decade termination shock that would arise in a world controlled by SRM alone (Figure S11), which is the worst-case scenario most often discussed in the literature (Parker and Irvine, 2018).

From the vantage point of $t_0 = 2020$, we can order the four scenarios described above based on their net present benefits: Yes-SRM > Term-Response > Term-SRM > No-SRM. However, adding damages due to CO_{2e} concentrations disadvantages Yes-SRM and Term-SRM relative to No-SRM and Term-Response, and adding damages due to the *rate* of warming disadvantages Term-SRM and Term-Response relative to No-SRM and Yes-SRM. If these costs are both sufficiently high, the ordering instead becomes: No-SRM > Yes-SRM > Term-Response > Term-SRM (see Figure S12 for the full sensitivity curves).

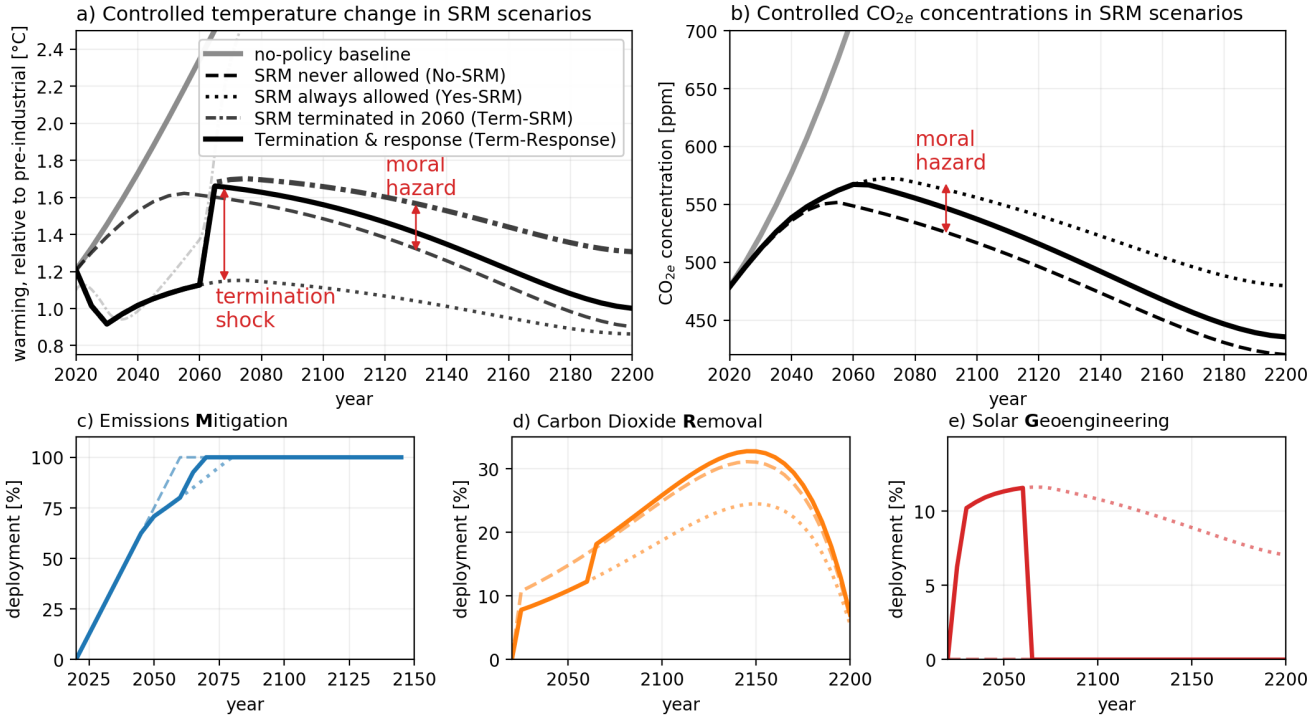

Figure 6: **Storyline B:** after $\Delta t = 40$ years of stabilizing global temperatures near present-day levels due in part to cooling by solar radiation modification (Yes-SRM; dotted lines), a surrogate policy decision-maker decides to abruptly terminate all SRM deployments (Term-SRM; dash-dotted lines). As SRM is terminated, temperatures rapidly rebound 0.6 °C (a "termination shock"), which is 0.05 °C warmer than in the counterfactual optimal trajectory in which SRM was never allowed (No-SRM, dashed lines) due to a 50 ppm increase in CO_{2e} attributed to deterred mitigation (a "moral hazard"). If the decision-maker responds to the termination by re-optimizing future control deployments (Term-Response; solid lines), however, they are able to eventually reduce CO_{2e} concentrations and temperatures back below pre-termination levels.

5 Discussion

Optimization of climate control in IAMs historically focused on trade-offs between emissions mitigation and climate suffering (Nordhaus, 1992; Tol, 1997), although numerous studies have also considered trade-offs between mitigation and alternative climate control strategies: adaptation (de Bruin et al., 2009), carbon dioxide removal (CDR; Kriegler et al., 2013), and solar radiation modification (SRM; Goes et al., 2011). Here, we explore trade-offs between all four of these approaches to climate control. The optimized deployment levels of the climate controls depend upon their respective marginal costs per marginal benefit, which themselves are a complicated function of: their deployment cost curves, the causal chain of processes by which they affect downstream climate damages, and the choice of value-dependent parameters. We developed MARGO, a multi-control and time-dependent numerical model of optimized climate policies, to quantitatively explore these trade-offs. In our optimized simulations, emissions mitigation emerges as the preferred climate control, although a time-dependent combination of substantial deployments of all four controls yields the most cost-beneficial and cost-effective climate outcomes.

For clarity of exposition, we present a fully deterministic version of the MARGO model. In actuality, key inputs such as the climate feedback parameter B and the damage function $D(T)$ are extremely uncertain. Propagation of these uncertainties through a convex damage function typically increases expected climate damages and strengthens the case for early and aggressive climate control (Wagner and Zeckhauser, 2016). Similarly, economic models with formulations of preferences that naturally incorporate uncertainty and risk yield imply more stringent controls (Cai and Lontzek, 2018; Daniel et al., 2019). Future work includes 1) extending MARGO to a stochastic programming approach that accounts for uncertainty in input parameters or stochastic climate dynamics (see Section S4.3) and 2) implementing a Bayesian policy response process where prior parameter distributions can be updated based on observed stochastic outcomes (e.g. Shayegh and Thomas, 2015) or improved parameter estimates from research developments (Hope, 2015).

Climate outcomes will inevitably differ from the anticipated outcomes of prescribed control policies, whether because of imperfect control deployments, inherent variability, or structural uncertainty and bias in projected climate outcomes. We propose a policy process by which a surrogate decision-maker responds to undesirable real world outcomes by sequentially re-optimizing prescriptions of future climate control deployments, as an improvement over previously-proposed strategies based on arbitrary decision trees (e.g. Goes et al., 2011; Hammitt et al., 1992; Lempert et al., 1996). We demonstrate the utility of this policy response process by quantifying its beneficial outcomes compared to alternative "static" policies in which the decision-maker adheres to their original strategy despite control shortfalls or changing policy constraints.

Presently, Intended Nationally Determined Contributions (INDCs) imply warming of 2.6–3.1 °C and thus will need to be strengthened at upcoming re-negotiations– and then actualized– to have a reasonable chance of meeting the Paris Agreement's goal of well below 2 °C of warming (Rogelj et al., 2016; United Nations Environment Programme, 2018; United Nations Framework Convention on Climate Change, 2015). Holz et al. (2018) explore plausible "ratcheting" scenarios in which mitigation efforts are iteratively increased relative to the INDCs, and optionally supplemented by varying levels of CDR, until expected warming remains below 1.5 °C in 2100. In Storyline A

(Section 4.2), we introduce a ratcheting process and show how a policy decision-maker might sequentially update their climate control prescriptions to compensate for realized climate control shortfalls, in order to salvage climate targets in an optimally cost-effective way.

Rapid warming due to an abrupt termination of SRM deployments is commonly considered one of the greatest risks of SRM (Parker and Irvine, 2018). Goes et al. (2011) show that substituting SRM for mitigation fails a cost-benefit test, especially when accounting for the risk of a termination shock. However, Bickel and Agrawal (2013) extend their analysis and argue that if decision-makers respond to termination by mitigating emissions (using a fixed decision-tree response), then SRM passes the cost-benefit over a much larger range of termination probabilities than in Goes et al. (2011). Helwegen et al. (2019) perform a similar analysis, but allow the decision-maker to respond with optimal changes in mitigation, and show that SRM deployments robustly enhance welfare, even when taking into account the risk of SRM termination triggering climate "tipping points". In Storyline B (Section 4.3), we extend this analysis by allowing decision-makers to optimally respond to SRM termination by also increasing CDR deployments, which yields substantial benefits relative to the scenario without a policy response. This storyline also provides quantitative evidence for a novel interaction between two processes that are independently considered major risks of SRM: the "termination shock" due to abrupt SRM termination is amplified by about 10% due to the "moral hazard" of mitigation deterred by decades of investment in SRM deployments.

Our assumption of a unitary surrogate decision-maker evidently avoids the complexities of a realistic decision-making process that involves multiple stake holders with conflicting interests. While some of these interactions are implicitly embedded in the two storylines described above, they could instead be explicitly included in a multi-agent extension of the MARGO model, in which the global climate response is the aggregated result of multiple agents exerting controls on the climate, according to their own diverging incentives (Emmerling et al., 2020; Heyen et al., 2019; Ricke et al., 2013).

The MARGO model fills the complexity gap between semi-analytic theoretical models (e.g. Deutch, 2019; Moreno-Cruz et al., 2018) and complicated IAMs (e.g. Hope, 2006; Nordhaus, 1992; Tol, 1997), as its dynamics are governed by only $N = 12$ intuitive free parameters but still produces quasi-realistic climate trajectories (see Section S3.2 and Table S1). We show how MARGO can be used to investigate the sensitivity of optimized climate control policies to poorly-known parameters, such as future control costs, and value-dependent parameters, such as the discount rate. We also demonstrate that MARGO can be modified to reproduce the qualitative results of other multi-control studies (e.g. Belaia et al. 2020; see Section S5) and hope that it will be a useful community tool for climate policy research, interactive teaching, and public outreach, and will help bridge the gaps between climate economists, scientists, policy decision-makers, and the public (Buck, 2010; Pindyck, 2017; Schneider, 1997; Stainforth and Calel, 2020). We encourage readers to interactively run the MARGO model themselves by visiting any of our web-apps at `https://github.com/ClimateMARGO/ClimateMARGO.jl/blob/master/Gallery.md`.

6 Acknowledgements

We thank Lyssa Freese and two anonymous reviewers for comments on earlier versions of the manuscript. We thank Fons van der Plas for leading the development of our online web-apps.

This material is based upon work supported by the National Science Foundation Graduate Research Fellowship Program under Grant No. 174530. Any opinions, findings, and conclusions or recommendations expressed in this material are those of the author(s) and do not necessarily reflect the views of the National Science Foundation.

7 Data availability

All data and figures used in the study can be found at `github.com/ClimateMARGO/MARGO-paper` and are readily reproduced or modified by the Jupyter notebooks therein.

References

Alley, R. B., Marotzke, J., Nordhaus, W. D., Overpeck, J. T., Peteet, D. M., Pielke, R. A., Pierrehumbert, R. T., Rhines, P. B., Stocker, T. F., Talley, L. D., and Wallace, J. M. (2003). Abrupt Climate Change. *Science*, 299(5615):2005–2010.

Arrow, K., Cropper, M., Gollier, C., Groom, B., Heal, G., Newell, R., Nordhaus, W., Pindyck, R., Pizer, W., Portney, P., Sterner, T., Tol, R. S. J., and Weitzman, M. (2013). Determining Benefits and Costs for Future Generations. *Science*, 341(6144):349–350. Publisher: American Association for the Advancement of Science Section: Policy Forum.

Azar, C. and Schneider, S. H. (2002). Are the economic costs of stabilising the atmosphere prohibitive? *Ecological Economics*, 42(1):73–80.

Belaia, M., Moreno-Cruz, J. B., and Keith, D. W. (2020). Optimal climate policy in three dimensions. Preprint.

Bezanson, J., Edelman, A., Karpinski, S., and Shah, V. (2017). Julia: A Fresh Approach to Numerical Computing. *SIAM Review*, 59(1):65–98.

Bickel, J. E. and Agrawal, S. (2013). Reexamining the economics of aerosol geoengineering. *Climatic Change*, 119(3):993–1006.

Brown, P. T., Moreno-Cruz, J., and Caldeira, K. (2020). Break-even year: a concept for understanding intergenerational trade-offs in climate change mitigation policy. *Environmental Research Communications*, 2(9):095002. Publisher: IOP Publishing.

Buck, H. J. (2010). What can geoengineering do for us? public participation and the new media landscape. In *Paper for workshop: The ethics of solar radiation management, 18 Oct 2010, University of Montana.*

Buck, H. J. (2012). Geoengineering: Re-making Climate for Profit or Humanitarian Intervention? *Development and Change*, 43(1):253–270. _eprint: https://onlinelibrary.wiley.com/doi/pdf/10.1111/j.1467-7660.2011.01744.x.

Burke, M., Hsiang, S. M., and Miguel, E. (2015). Global non-linear effect of temperature on economic production. *Nature*, 527(7577):235–239. Number: 7577 Publisher: Nature Publishing Group.

Cai, Y. and Lontzek, T. S. (2018). The Social Cost of Carbon with Economic and Climate Risks. *Journal of Political Economy*, 127(6):2684–2734. Publisher: The University of Chicago Press.

Caldeira, K., Bala, G., and Cao, L. (2013). The Science of Geoengineering. *Annual Review of Earth and Planetary Sciences*, 41(1):231–256. _eprint: https://doi.org/10.1146/annurev-earth-042711-105548.

Caldeira, K. and Ricke, K. L. (2013). Prudence on solar climate engineering. *Nature Climate Change*, 3(11):941–941. Number: 11 Publisher: Nature Publishing Group.

Christensen, P., Gillingham, K., and Nordhaus, W. (2018). Uncertainty in forecasts of long-run economic growth. *Proceedings of the National Academy of Sciences*, 115(21):5409–5414.

Clarke, L. E., Jiang, K., Akimoto, K., Babiker, M., Blanford, G. J., Fisher-Vanden, K., Hourcade, J.-C., Krey, V., Kriegler, E., Loschel, A., et al. (2014). Assessing Transformation Pathways. In: Climate Change 2014: Mitigation of Climate Change. Contribution of Working Group III to the Fifth Assessment Report of the Intergovernmental Panel on Climate Change. Technical report.

Council, N. R. et al. (1991). Policy implications of greenhouse warming. In *Report of the Committee on Science, Engineering and Public Policy*, page 127. National Academy Press Washington, DC.

Crutzen, P. J. (2006). Albedo Enhancement by Stratospheric Sulfur Injections: A Contribution to Resolve a Policy Dilemma? *Climatic Change*, 77(3):211.

Daniel, K. D., Litterman, R. B., and Wagner, G. (2019). Declining CO2 price paths. *Proceedings of the National Academy of Sciences*, 116(42):20886–20891. Publisher: National Academy of Sciences Section: Social Sciences.

de Bruin, K. C., Dellink, R. B., and Tol, R. S. J. (2009). AD-DICE: an implementation of adaptation in the DICE model. *Climatic Change*, 95(1):63–81.

Deutch, J. M. (2019). Joint allocation of climate control mechanisms is the cheapest way to reduce global climate damage. *MIT Center for Energy and Environmental Policy Research Working Paper Series*.

Dow, K., Berkhout, F., Preston, B. L., Klein, R. J. T., Midgley, G., and Shaw, M. R. (2013). Limits to adaptation. *Nature Climate Change*, 3(4):305–307. Number: 4 Publisher: Nature Publishing Group.

Emmerling, J., Kornek, U., Bosetti, V., and Lessmann, K. (2020). Climate thresholds and heterogeneous regions: Implications for coalition formation. *The Review of International Organizations*.

Flegal, J. A. and Gupta, A. (2018). Evoking equity as a rationale for solar geoengineering research? Scrutinizing emerging expert visions of equity. *International Environmental Agreements: Politics, Law and Economics*, 18(1):45–61.

Flegal, J. A., Hubert, A.-M., Morrow, D. R., and Moreno-Cruz, J. B. (2019). Solar Geoengineering: Social Science, Legal, Ethical, and Economic Frameworks. *Annual Review of Environment and Resources*, 44(1):399–423. _eprint: https://doi.org/10.1146/annurev-environ-102017-030032.

Fuss, S., Canadell, J. G., Peters, G. P., Tavoni, M., Andrew, R. M., Ciais, P., Jackson, R. B., Jones, C. D., Kraxner, F., Nakicenovic, N., Quéré, C. L., Raupach, M. R., Sharifi, A., Smith, P., and Yamagata, Y. (2014). Betting on negative emissions. *Nature Climate Change*, 4(10):850–853. Number: 10 Publisher: Nature Publishing Group.

Fuss, S., Lamb, W. F., Callaghan, M. W., Hilaire, J., Creutzig, F., Amann, T., Beringer, T., Garcia, W. d. O., Hartmann, J., Khanna, T., Luderer, G., Nemet, G. F., Rogelj, J., Smith, P., Vicente, J. L. V., Wilcox, J., Dominguez, M. d. M. Z., and Minx, J. C. (2018). Negative emissions—Part 2: Costs, potentials and side effects. *Environmental Research Letters*, 13(6):063002. Publisher: IOP Publishing.

Geoffroy, O., Saint-Martin, D., Olivié, D. J. L., Voldoire, A., Bellon, G., and Tytéca, S. (2012). Transient Climate Response in a Two-Layer Energy-Balance Model. Part I: Analytical Solution and Parameter Calibration Using CMIP5 AOGCM Experiments. *Journal of Climate*, 26(6):1841–1857. Publisher: American Meteorological Society.

Glanemann, N., Willner, S. N., and Levermann, A. (2020). Paris Climate Agreement passes the cost-benefit test. *Nature Communications*, 11(1):1–11. Number: 1 Publisher: Nature Publishing Group.

Global Commission on Adaptation (2019). Adapt now: A global call for leadership on climate resilience. Technical report.

Glotter, M. J., Pierrehumbert, R. T., Elliott, J. W., Matteson, N. J., and Moyer, E. J. (2014). A simple carbon cycle representation for economic and policy analyses. *Climatic Change*, 126(3):319–335.

Goes, M., Tuana, N., and Keller, K. (2011). The economics (or lack thereof) of aerosol geoengineering. *Climatic Change*, 109(3):719–744.

Haerlin, B. and Parr, D. (1999). How to restore public trust in science. *Nature*, 400(6744):499–499. Number: 6744 Publisher: Nature Publishing Group.

Hammitt, J. K., Lempert, R. J., and Schlesinger, M. E. (1992). A sequential-decision strategy for abating climate change. *Nature*, 357(6376):315–318. Number: 6376 Publisher: Nature Publishing Group.

Helwegen, K. G., Wieners, C. E., Frank, J. E., and Dijkstra, H. A. (2019). Complementing CO_2 emission reduction by solar radiation management might strongly enhance future welfare. *Earth System Dynamics*, 10(3):453–472. Publisher: Copernicus GmbH.

Heyen, D., Horton, J., and Moreno-Cruz, J. (2019). Strategic implications of counter-geoengineering: Clash or cooperation? *Journal of Environmental Economics and Management*, 95:153–177.

Holz, C., Siegel, L. S., Johnston, E., Jones, A. P., and Sterman, J. (2018). Ratcheting ambition to limit warming to 1.5\hspace0.167em°C–trade-offs between emission reductions and carbon dioxide removal. *Environmental Research Letters*, 13(6):064028. Publisher: IOP Publishing.

Hope, C. (2006). The marginal impact of co2 from page2002: an integrated assessment model incorporating the ipcc's five reasons for concern. *Integrated assessment*, 6(1).

Hope, C. (2015). The $10 trillion value of better information about the transient climate response. *Philosophical Transactions. Series A, Mathematical, Physical, and Engineering Sciences*, 373(2054).

Kelleher, J. P. and Wagner, G. (2019). Ramsey discounting calls for subtracting climate damages from economic growth rates. *Applied Economics Letters*, 26(1):79–82. Publisher: Routledge _eprint: https://doi.org/10.1080/13504851.2018.1438581.

Kellogg, W. W. and Schneider, S. H. (1974). Climate Stabilization: For Better or for Worse? *Science*, 186(4170):1163–1172. Publisher: American Association for the Advancement of Science Section: Articles.

Koomey, J. (2013). Moving beyond benefit–cost analysis of climate change. *Environmental Research Letters*, 8(4):041005. Publisher: IOP Publishing.

Kriegler, E., Edenhofer, O., Reuster, L., Luderer, G., and Klein, D. (2013). Is atmospheric carbon dioxide removal a game changer for climate change mitigation? *Climatic Change*, 118(1):45–57.

Lacey, J., Howden, M., Cvitanovic, C., and Colvin, R. M. (2018). Understanding and managing trust at the climate science–policy interface. *Nature Climate Change*, 8(1):22–28. Number: 1 Publisher: Nature Publishing Group.

Lempert, R. J., Schlesinger, M. E., and Bankes, S. C. (1996). When we don't know the costs or the benefits: Adaptive strategies for abating climate change. *Climatic Change*, 33(2):235–274.

Lickley, M., Cael, B. B., and Solomon, S. (2019). Time of Steady Climate Change. *Geophysical Research Letters*, 46(10):5445–5451. _eprint: https://agupubs.onlinelibrary.wiley.com/doi/pdf/10.1029/2018GL081704.

Lin, A. C. (2013). Does Geoengineering Present a Moral Hazard. *Ecology Law Quarterly*, 40(3):i–712.

Manabe, S. and Wetherald, R. T. (1967). Thermal equilibrium of the atmosphere with a given distribution of relative humidity. *Journal of the Atmospheric Sciences*, 24(3):241–259.

Matthews, H. D. and Caldeira, K. (2007). Transient climate–carbon simulations of planetary geoengineering. *Proceedings of the National Academy of Sciences*, 104(24):9949–9954. Publisher: National Academy of Sciences Section: Physical Sciences.

Matthews, H. D. and Caldeira, K. (2008). Stabilizing climate requires near-zero emissions. *Geophysical Research Letters*, 35(4). _eprint: https://agupubs.onlinelibrary.wiley.com/doi/pdf/10.1029/2007GL032388.

McClellan, J., Keith, D. W., and Apt, J. (2012). Cost analysis of stratospheric albedo modification delivery systems. *Environmental Research Letters*, 7(3):034019. Publisher: IOP Publishing.

McLaren, D. (2016). Mitigation deterrence and the "moral hazard" of solar radiation management. *Earth's Future*, 4(12):596–602. _eprint: https://agupubs.onlinelibrary.wiley.com/doi/pdf/10.1002/2016EF000445.

Modak, A., Bala, G., Cao, L., and Caldeira, K. (2016). Why must a solar forcing be larger than a CO 2 forcing to cause the same global mean surface temperature change? *Environmental Research Letters*, 11(4):044013. Publisher: IOP Publishing.

Moore, F. C. and Diaz, D. B. (2015). Temperature impacts on economic growth warrant stringent mitigation policy. *Nature Climate Change*, 5(2):127–131. Number: 2 Publisher: Nature Publishing Group.

Moreno-Cruz, J., Wagner, G., and Keith, D. (2018). An Economic Anatomy of Optimal Climate Policy. SSRN Scholarly Paper ID 3001221, Social Science Research Network, Rochester, NY.

Nordhaus, W. and Sztorc, P. (2013). Dice 2013r: Introduction and user's manual. *Yale University and the National Bureau of Economic Research, USA*.

Nordhaus, W. D. (1992). An Optimal Transition Path for Controlling Greenhouse Gases. *Science*, 258(5086):1315–1319. Publisher: American Association for the Advancement of Science Section: Articles.

Parker, A. and Irvine, P. J. (2018). The Risk of Termination Shock From Solar Geoengineering. *Earth's Future*, 6(3):456–467. _eprint: https://agupubs.onlinelibrary.wiley.com/doi/pdf/10.1002/2017EF000735.

Parson, E. A. (2017). Opinion: Climate policymakers and assessments must get serious about climate engineering. *Proceedings of the National Academy of Sciences*, 114(35):9227–9230. Publisher: National Academy of Sciences Section: Opinion.

Parson, E. A. and Keith, D. W. (2013). End the Deadlock on Governance of Geoengineering Research. *Science*, 339(6125):1278–1279. Publisher: American Association for the Advancement of Science Section: Policy Forum.

Peters, G. P., Andrew, R. M., Canadell, J. G., Friedlingstein, P., Jackson, R. B., Korsbakken, J. I., Quéré, C. L., and Peregon, A. (2020). Carbon dioxide emissions continue to grow amidst slowly emerging climate policies. *Nature Climate Change*, 10(1):3–6. Number: 1 Publisher: Nature Publishing Group.

Peters, G. P., Andrew, R. M., Canadell, J. G., Fuss, S., Jackson, R. B., Korsbakken, J. I., Le Quéré, C., and Nakicenovic, N. (2017). Key indicators to track current progress and future ambition of the Paris Agreement. *Nature Climate Change*, 7(2):118–122. Number: 2 Publisher: Nature Publishing Group.

Pindyck, R. S. (2017). The Use and Misuse of Models for Climate Policy. *Review of Environmental Economics and Policy*, 11(1):100–114. Publisher: Oxford Academic.

Ramsey, F. P. (1928). A Mathematical Theory of Saving. *The Economic Journal*, 38(152):543–559. Publisher: [Royal Economic Society, Wiley].

Revelle, R., Broecker, W., Craig, H., Kneeling, C., and Smagorinsky, J. (1965). Restoring the quality of our environment: report of the environmental pollution panel. Atmospheric carbon dioxide. *President's Science Advisory Committee, United States, US Government Printing Office: Washington, DC*.

Riahi, K., van Vuuren, D. P., Kriegler, E., Edmonds, J., O'Neill, B. C., Fujimori, S., Bauer, N., Calvin, K., Dellink, R., Fricko, O., Lutz, W., Popp, A., Cuaresma, J. C., Kc, S., Leimbach, M., Jiang, L., Kram, T., Rao, S., Emmerling, J., Ebi, K., Hasegawa, T., Havlik, P., Humpenöder, F., Da Silva, L. A., Smith, S., Stehfest, E., Bosetti, V., Eom, J., Gernaat, D., Masui, T., Rogelj, J., Strefler, J., Drouet, L., Krey, V., Luderer, G., Harmsen, M., Takahashi, K., Baumstark, L., Doelman, J. C., Kainuma, M., Klimont, Z., Marangoni, G., Lotze-Campen, H., Obersteiner, M., Tabeau, A., and Tavoni, M. (2017). The Shared Socioeconomic Pathways and their energy, land use, and greenhouse gas emissions implications: An overview. *Global Environmental Change*, 42:153–168.

Ricke, K. L., Moreno-Cruz, J. B., and Caldeira, K. (2013). Strategic incentives for climate geoengineering coalitions to exclude broad participation. *Environmental Research Letters*, 8(1):014021. Publisher: IOP Publishing.

Robock, A., Oman, L., and Stenchikov, G. L. (2008). Regional climate responses to geoengineering with tropical and Arctic SO2 injections. *Journal of Geophysical Research: Atmospheres*, 113(D16). _eprint: https://agupubs.onlinelibrary.wiley.com/doi/pdf/10.1029/2008JD010050.

Rogelj, J., Elzen, M. d., Höhne, N., Fransen, T., Fekete, H., Winkler, H., Schaeffer, R., Sha, F., Riahi, K., and Meinshausen, M. (2016). Paris Agreement climate proposals need a boost to keep warming well below 2 °C. *Nature*, 534(7609):631–639. Number: 7609 Publisher: Nature Publishing Group.

Schneider, S. H. (1989). The Greenhouse Effect: Science and Policy. *Science*, 243(4892):771–781. Publisher: American Association for the Advancement of Science Section: Articles.

Schneider, S. H. (1997). Integrated assessment modeling of global climate change: Transparent rational tool for policy making or opaque screen hiding value-laden assumptions? *Environmental Modeling & Assessment*, 2(4):229–249.

Schäfer, S., Irvine, P. J., Hubert, A.-M., Reichwein, D., Low, S., Stelzer, H., Maas, A., and Lawrence, M. G. (2013). Field tests of solar climate engineering. *Nature Climate Change*, 3(9):766–766. Number: 9 Publisher: Nature Publishing Group.

Shayegh, S. and Thomas, V. M. (2015). Adaptive stochastic integrated assessment modeling of optimal greenhouse gas emission reductions. *Climatic Change*, 128(1):1–15.

Shepherd, T. G., Boyd, E., Calel, R. A., Chapman, S. C., Dessai, S., Dima-West, I. M., Fowler, H. J., James, R., Maraun, D., Martius, O., Senior, C. A., Sobel, A. H., Stainforth, D. A., Tett, S. F. B., Trenberth, K. E., van den Hurk, B. J. J. M., Watkins, N. W., Wilby, R. L., and Zenghelis, D. A. (2018). Storylines: an alternative approach to representing uncertainty in physical aspects of climate change. *Climatic Change*, 151(3):555–571.

Solomon, S., Plattner, G.-K., Knutti, R., and Friedlingstein, P. (2009). Irreversible climate change due to carbon dioxide emissions. *Proceedings of the National Academy of Sciences*, 106(6):1704–1709. Publisher: National Academy of Sciences Section: Physical Sciences.

Solow, R. M. (1974). The Economics of Resources or the Resources of Economics. *The American Economic Review*, 64(2):1–14. Publisher: American Economic Association.

Stainforth, D. A. and Calel, R. (2020). New priorities for climate science and climate economics in the 2020s. *Nature Communications*, 11(1):3864. Number: 1 Publisher: Nature Publishing Group.

Steffen, W., Rockström, J., Richardson, K., Lenton, T. M., Folke, C., Liverman, D., Summerhayes, C. P., Barnosky, A. D., Cornell, S. E., Crucifix, M., Donges, J. F., Fetzer, I., Lade, S. J., Scheffer, M., Winkelmann, R., and Schellnhuber, H. J. (2018). Trajectories of the Earth System in the Anthropocene. *Proceedings of the National Academy of Sciences of the United States of America*, 115(33):8252–8259.

Stern, N., Stern, N. H., and Treasury, G. B. (2007). *The Economics of Climate Change: The Stern Review*. Cambridge University Press.

Talati, S. and Higgins, P. (2019). Policy sector perspectives on geoengineering risk and governance. *Journal of Science Policy & Governance*, 14.

Tol, R. S. (1997). On the optimal control of carbon dioxide emissions: an application of FUND. *Environmental Modeling & Assessment*, 2(3):151–163.

Tol, R. S. J. (2003). Is the Uncertainty about Climate Change too Large for Expected Cost-Benefit Analysis? *Climatic Change*, 56(3):265–289.

United Nations Environment Programme (2018). The emissions gap report 2020. Technical report.

United Nations Framework Convention on Climate Change (2015). Paris agreement. Article 2(a). `https://unfccc.int/process-and-meetings/the-paris-agreement/theparis-agreement`.

Victor, D. G., Morgan, M. G., Apt, F., and Steinbruner, J. (2009). The Geoengineering Option - A Last Resort against Global Warming Essay. *Foreign Affairs*, 88(2):64–76.

Visioni, D., Pitari, G., and Aquila, V. (2017). Sulfate geoengineering: a review of the factors controlling the needed injection of sulfur dioxide. *Atmospheric Chemistry and Physics*, 17(6):3879–3889. Publisher: Copernicus GmbH.

Wagner, G. and Zeckhauser, R. J. (2016). Confronting Deep and Persistent Climate Uncertainty. SSRN Scholarly Paper ID 2818035, Social Science Research Network, Rochester, NY.

Weyant, J. (2017). Some Contributions of Integrated Assessment Models of Global Climate Change. *Review of Environmental Economics and Policy*, 11(1):115–137. Publisher: Oxford Academic.

Wächter, A. and Biegler, L. T. (2006). On the implementation of an interior-point filter line-search algorithm for large-scale nonlinear programming. *Mathematical Programming*, 106(1):25–57.

Supplementary Information for "A simple model for assessing climate control trade-offs and responding to unanticipated climate outcomes"

Henri F. Drake*[1,2], Ronald L. Rivest[1], Alan Edelman[1], and John Deutch[1]

[1] *Massachusetts Institute of Technology, Cambridge, MA, USA*

[2] *MIT-WHOI Joint Program in Oceanography/Applied Ocean Science & Engineering, Cambridge and Woods Hole, MA, USA*

Contents

S1 Description and validation of MARGO's geophysical climate module

S1.1 The two-box Energy Balance Model (EBM)

Zero-dimensional energy balance box models are a common tool for simulating Earth's complex planetary climate and its response to anthropogenic radiative forcing. These models provided the earliest projections of anthropogenic global warming (Hausfather et al., 2020) and are still used as simple and inexpensive emulators of more complicated and computationally expensive three-dimensional General Circulation Models (Geoffroy et al., 2012). In the two-box linear energy balance model considered here, the evolution of the global-mean near-surface temperature anomaly (relative to the initial time $t_0 = 2020$) is governed by two coupled ordinary differential equations (Gregory, 2000; Held et al., 2010):

$$C_U \frac{\mathrm{d}T}{\mathrm{d}t} = -BT - \kappa(T - T_D) + F(t), \tag{S1}$$

$$C_D \frac{\mathrm{d}T_D}{\mathrm{d}t} = \kappa(T - T_D), \tag{S2}$$

where (S1) represents the upper ocean box with average temperature anomaly T, and (S2) represents the deep ocean box with an average temperature T_D. Solutions to equations (S1) and (S2) will hereafter be referred to as Energy Balance Models (EBMs). The near-surface atmosphere exchanges heat anomalies rapidly with the upper ocean and thus the global-mean near-surface air temperature, MARGO's proxy variable for the magnitude of climate change, is also given by T. The physical model parameters are: the upper ocean heat capacity $C_U = 7.3\,\mathrm{W\,yr\,m^{-2}\,K^{-1}}$ (including a negligible contribution $C_A \ll C_U$ from the atmospheric column); the deep ocean heat capacity $C_D = 106\,\mathrm{W\,yr\,m^{-2}\,K^{-1}}$; the climate feedback parameter $B = 1.13\,\mathrm{W\,m^{-2}\,K^{-1}}$; and the ocean heat uptake rate $\kappa = 0.73\,\mathrm{W\,m^{-2}\,K^{-1}}$. These parameter values are taken from the multi-model mean of values diagnosed uniquely from simulations of 16 CMIP5 models (Geoffroy et al., 2012). The radiative forcing and temperature anomalies at $t_0 = 2020$, relative to preindustrial, are $F(t_0) - F(t_{\mathrm{PI}}) = 3\,\mathrm{W\,m^{-2}}$ and $T_0 \equiv T(t_0) - T(t_{\mathrm{PI}}) = 1.1\,\mathrm{K}$, where we set $F_0 \equiv F(t_0) = 0\,\mathrm{W\,m^{-2}}$ and $T(t_{\mathrm{PI}}) = 0\,\mathrm{K}$ for convenience.

The $\kappa(T - T_D)$ term models heat exchange between the upper ocean and deep ocean boxes. Summing (S1) and (S2), we get the global energy balance equation

$$C_U \frac{\mathrm{d}T}{\mathrm{d}t} + C_D \frac{\mathrm{d}T_D}{\mathrm{d}t} = F(t) - BT, \tag{S3}$$

where the left hand side is the rate of change of Earth's heat content; $F(t)$ is the anomalous radiative forcing of the system at top-of-atmosphere (TOA); $BT(t)$ is the anomalous outgoing radiation at TOA; and the $\kappa(T - T_D)$ vanishes in the net because it only exchanges heat between the two boxes.

S1.2 The Deep-layer Energy Balance Model (DEBM) approximation

For most policy-relevant climate change applications, the EBM equations (S1 & S2) are unnecessary complicated. In particular, if the anthropogenic forcing $F(t)$ varies on timescales longer than the fast relaxation timescale $\tau_U = C_U/(B + \kappa) = 4\,\mathrm{years}$, as is the case in realistic scenarios of anthropogenic forcing, we can ignore the

time-dependence in the upper ocean equation (S1) and approximate

$$T \approx \frac{F + \kappa T_D}{B + \kappa}. \tag{S4}$$

The evolution of the deep ocean heat content thus simplifies to

$$C_D \frac{\mathrm{d}T_D}{\mathrm{d}t} \approx -\frac{B\kappa}{B+\kappa} T_D + \frac{\kappa}{B+\kappa} F, \tag{S5}$$

and occurs on a slower timescale $\tau_D \equiv \frac{C_D}{B}\frac{B+\kappa}{\kappa} = 240\,\text{years}$ (Held et al., 2010). Plugging the exact Green's Function solution to the approximate equation (S5) back into (S4) gives the closed-form solution

$$T(t) - T_0 = \frac{F(t)}{B+\kappa} + \frac{\kappa}{B}\frac{1}{(B+\kappa)} \int_{t_0}^{t} \frac{e^{-(t-t')/\tau_D}}{\tau_D} F(t')\,\mathrm{d}t', \tag{S6}$$

hereafter referred as the Deep-layer Energy Balance Model (DEBM). The evolution of the controlled temperature anomaly (eq. 5; Figure 2d) has the same form but is instead driven by the controlled net radiative forcing $F_{M,R,G}$.

We identify the first term on the right hand side of (S6) and (5) as the transient (fast) climate response (Gregory and Forster, 2008), which dominates for $t - t_0 \ll \tau_D$, while the second term is a recalcitrant (slow) response due to a weakening of ocean heat uptake as the deep ocean comes to equilibrium with the upper ocean (Held et al., 2010). While the contribution of the recalcitrant component to historical warming is thought to be small, it contributes significantly to 21st century and future warming (Gregory and Forster, 2008; Held et al., 2010). We here assume a "cold-start" where the deep ocean temperature anomaly T_D is assumed to be zero, but this term could easily be added to the right hand side of (S4) if warranted by the application.

The behavior of the model on short and long timescales is illustrated by applying it to the canonical climate change experiment in which CO_2 concentrations increase at 1% per year until doubling (Figure S1). Warming rapidly increases until shortly after the forcing stabilizes at the time of doubling $t = t_{2\times}$, where $t_{2\times} - t_0 \approx 70\,\text{years} \ll \tau_D$, and $F_{2\times} = a\ln\left(\frac{2c_0}{c_0}\right) = a\ln(2)$. Since $t_{2\times} - t_0 \ll \tau_D$, the warming at $t_{2\times}$ is dominated by the fast response and the Transient Climate Response is $\text{TCR} = T(t_{2\times}) \approx \frac{F_{2\times}}{B+\kappa} = 1.9\,^{\circ}\text{C}$. As time advances further, the slow mode grows and eventually and eventually warming asymptotes to the Equilibrium Climate Sensitivity, $\text{ECS} = \frac{F_{2\times}}{B} = 3.1\,^{\circ}\text{C} > \text{TCS}$, as $t - t_0 \gg \tau_D$.

S1.3 Comparison of the DEBM and EBMs with CMIP5 GCM simulations under RCP8.5-like extreme forcing

We validate MARGO's DEBM by comparing it to an ensemble of 35 models from the Coupled Model Intercomparison Project 5 (CMIP5) under the RCP8.5 forcing scenario. We also compare MARGO's DEBM solution to an EBM with identical parameters values, and to an EBM calibrated with DICE's parameter values as a point of reference.

First, we construct an idealized forcing scenario that is meant to appromximate RCP8.5 (Riahi et al., 2007) and its extension beyond 2100, ECP8.5 (Meinshausen et al., 2011). In our scenario, baseline CO_{2e} emissions: 1) increase exponentially with a growth rate of $1/37\,\text{years}^{-1}$ to reach a maximum of $410\,\text{GtCO}_{2e}$/year in 2100, approximately

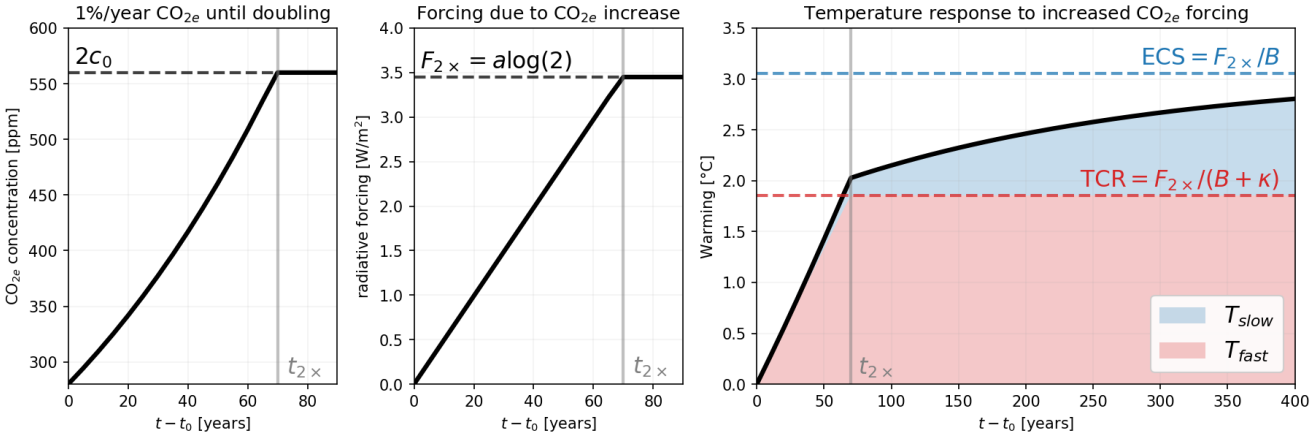

Supplementary Figure S1: Temperature response of MARGO's Deep-layer EBM to a compound 1% per year increase in CO_{2e} concentrations until doubling, decomposed into its fast (red shading) and slow modes (blue shading).

7 times present-day emissions; 2) plateau between 2100 and 2120; and 3) decrease linearly to zero between 2120 and 2200 (Figure S2a). As a result, CO_{2e} concentrations increase exponentially from the preindustrial value $c_0 = 280\,\text{ppm}$ in 1850 to 1400 ppm in 2100. In the extended scenario ECP8.5, CO_{2e} concentrations continue to grow until stabilizing at 3000 ppm in 2200[1] (Figure S2b). These increases in CO_{2e} drive a radiative forcing which increases to $F = 8.5\,\text{W/m}^2$ by 2100 and stabilizes at $F = 12\,\text{W/m}^2$ by 2200 (Figure S2c). The forcing timeseries constructed here approximates the RCP8.5 and ECP8.5 scenarios reasonably well: compare our Figure S2c with Figure 4 of Meinshausen et al (2011; Meinshausen et al., 2011).

We subject the MARGO DEBM to the RCP8.5-like scenario introduced above and almost exactly recover the multi-model-mean warming from the CMIP5 ensemble under RCP8.5 (Figure S2d, solid black and blue lines). The excellent agreement is not surprising, given that we tuned MARGO's DEBM with parameter values that were themselves calibrated to different experiments in the very same CMIP5 model ensemble (Geoffroy et al., 2012). The DEBM (solid black line) introduces small errors relative to the exact EBM solution with identical parameters under the ECP8.5 forcing scenario, as the exact response is effectively delayed by the short upper-ocean timescale $\tau_U = 4\,\text{years}$ relative to the DEBM (solid black line). If we dramatically reduce the deep ocean heat uptake rate κ, as is customary in IAMs (Calel and Stainforth, 2016), then the model 1) equilibrates much too quickly with the instantaneous forcing and 2) underestimates recalcitrant changes that occurs long after the radiative forcing is stabilized (Figure S2e, dotted black line).

The EBMs implemented as physical climate modules in IAMs are typically calibrated to either historical warming or simulated 21st Century warming in General Circulation Models under a series of emissions scenarios. However, such a calibration may produce unphysical results on shorter ($\ll 100\,\text{years}$) or longer ($\gg 100$) timescales. Following Calel and Stainforth (2016), Figure S2e shows how the DICE model's EBM calibration exhibits small errors for 21st Century warming but large errors on longer timescales. The climate physics-based calibration used here (Geoffroy et al., 2012) correctly includes the role of deep-ocean heat uptake in delaying warming and is more realistic than

[1]In the original definition of the ECP8.5 scenario (Meinshausen et al., 2011), much of these CO_{2e} increases are the result of increases in other gases such as Methane, Nitrous Oxide, and Hydrofluorocarbons, whose dynamics are poorly represented by CO_2 equivalence.

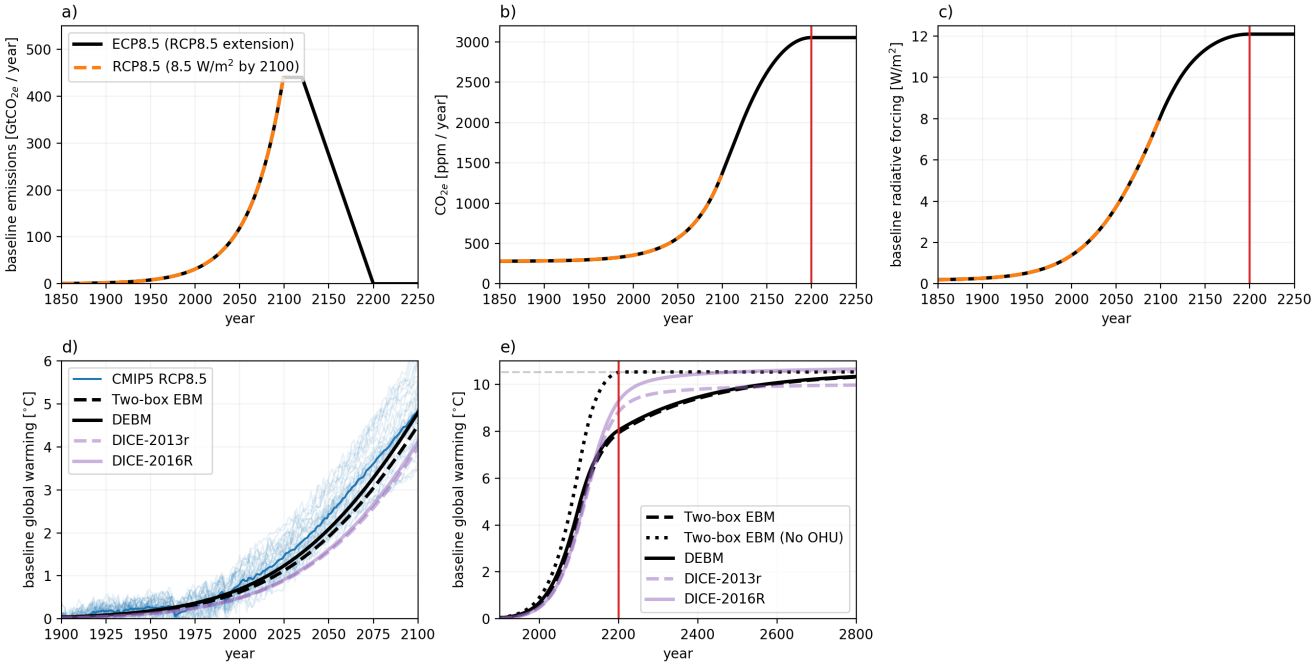

Supplementary Figure S2: Validation of the 21st Century and equilibrium responses of the Deep-layer Energy Balance Model (DEBM) used in MARGO. a) Baseline CO_{2e} emissions, b) concentrations, and c) radiative forcing in an RCP8.5-like scenario (dashed orange line) and its extension beyond 2100 (ECP8.5; solid black line). d) The transient temperature response of CMIP5 models to the RCP8.5 forcing scenario (thin blue lines for individual models; thick blue line for multi-model mean) and of MARGO's DEBM (solid black line) to the RCP8.5-like scenario. The dashed black line shows the exact solution to the two-layer equations (S1) and (S2) with the same parameter values (Geoffroy 2013; Geoffroy et al., 2012) as the approximate solution (eq. S6) used in MARGO's DEBM. e) The equilibrium temperature response to the ECP8.5 scenario for: MARGO's DEBM (solid) and the Geoffroy et al. (2012)-calibrated EBM, with (dashed black line) and without (dotted line) ocean heat uptake κ (OHU). Omitting OHU, i.e. setting $\kappa = 0$, is equivalent to considering a one-box upper-ocean model. The vertical red lines delineate 2200, the year in which the ECP8.5 emissions reach net zero and concentrations are stabilized. The transparent purple lines in d) and e) show the temperature response of the EBM calibrated with parameter values from DICE-2013r (Nordhaus and Sztorc, 2013) and DICE-2016R Nordhaus (2017), respectively, following Calel and Stainforth (2016).

those of widely-used IAMs (Calel and Stainforth, 2016).

S1.4 Comparison of the DEBM with various EBM solutions under rapidly-varying SRM forcings

The possibility for rapid deployment or termination of solar radiation modification (SRM) requires that climate-economic models used to study SRM scenarios be able to also respond realistically to rapidly-varying radiative forcings. We compare MARGO's DEBM to two alternative EBM formulations used in IAMs, by assessing their simulated response to an idealized forcing scenario in which SRM is rapidly deployed in 2020, held constant until 2060, and then abruptly terminated, while CO_{2e} forcing increases without control (Figure S3a; see Scenario B in Section 4). The ground-truth reference is the exact solution of the two-box EBM with Geoffroy et al. 2012's

physically-calibrated parameter values.

MARGO's DEBM (Figure S3b) yields a reasonably accurate temperature response for a short-timestep $\delta t = 1$ year, but leads the exact solution by about τ_U due to the omission of upper-ocean thermal inertia. Conveniently, speeding up MARGO by increasing the timestep to $\delta t = 5$ years decreases bias by delaying the response to short-term forcing changes by $\delta t \approx \tau_U$. Longer timesteps unrealistically delay the warming even further, but are numerically stable and still eventually produce the correct warming (and warming rates).

For short timesteps $\delta t < \tau_U$, the first-order forward finite-difference solution to the two-layer EBM (e.g. as used in DICE) is extremely accurate (Figure S3d). However, as δt is increased above $\tau_U = 4$ years, this naïve numerical solution becomes numerically unstable. Since performance is a major goal of the ClimateMARGO.jl implementation, the DEBM formulation is more desirable since it remains numerically stable for $\delta = 10$ to 30 years, which reduces the run time of the optimization and still yields quantitatively similar results.

The DICE-calibrated EBMs (both 2013 and 2016 versions) produce an unrealistically delayed (and slow) response due to its unrealistically high upper ocean thermal inertia (Figure S3c). As in Goes et al. (2011) and Helwegen et al. (2019)'s analyses, the DICE EBM should be replaced by a geophysical climate module that better represents the fast climate mode when using DICE to explore SRM scenarios. For example, Helwegen et al. (2019) use temperature impulse response functions proposed by MacMartin and Kravitz (2016), which is well described by exponential decay with a timescale of 4 years and corresponds exactly to the fast upper-ocean mode in Geoffroy et al. (2012)'s Greens Function solution to the two-layer EBM described above.

S2 Tuning of control costs

The scaling costs for the four controls used in the present study are based on prior research but ultimately subjective; we here describe our rationale for choosing the parameter values. The reference costs here are as a function of cumulative deployment; their derivatives $\mathcal{M}_\alpha = \dfrac{\mathrm{d}\,(\mathcal{C}_\alpha \alpha^2)}{\mathrm{d}\,\alpha}$ yield the marginal costs (multiply the cost of full deployment by 2 to get the marginal scaling cost). We remind the reader that the purpose of the MARGO model is to reveal insights about trade offs between the multiple controls and the dependence of model results on structural and parameteric choices, not to make quantitative predictions or provide detailed policy recommendations. The interested reader can choose their own parameter values and see how the results change by visiting our gallery of web-browser applications at `github.com/ClimateMARGO/ClimateMARGO.jl/gallery.md`.

S2.1 Mitigation

The costs of mitigation are set according to the Working Group III contribution to Intergovernmental Panel on Climate Change's Fifth Assessment Report (Clarke et al., 2014). In aggressive mitigation scenarios where CO_{2e} emissions decrease 78% to 118% by 2100, they estimate abatement costs of about 2% of GWP (see their Figure 6.21, panel f). However, we would like the cost of mitigation to scale with the baseline emissions q, instead, since these may become decoupled to GWP for reasons independent of climate policy. Thus, we set the scaling cost of mitigation controls to $\mathcal{C}_M = \tilde{\mathcal{C}}_M q$, where the hypothetical cost of mitigating all 2020 emissions, q_0, is $\mathcal{C}_M = 2\%$ of the GWP in

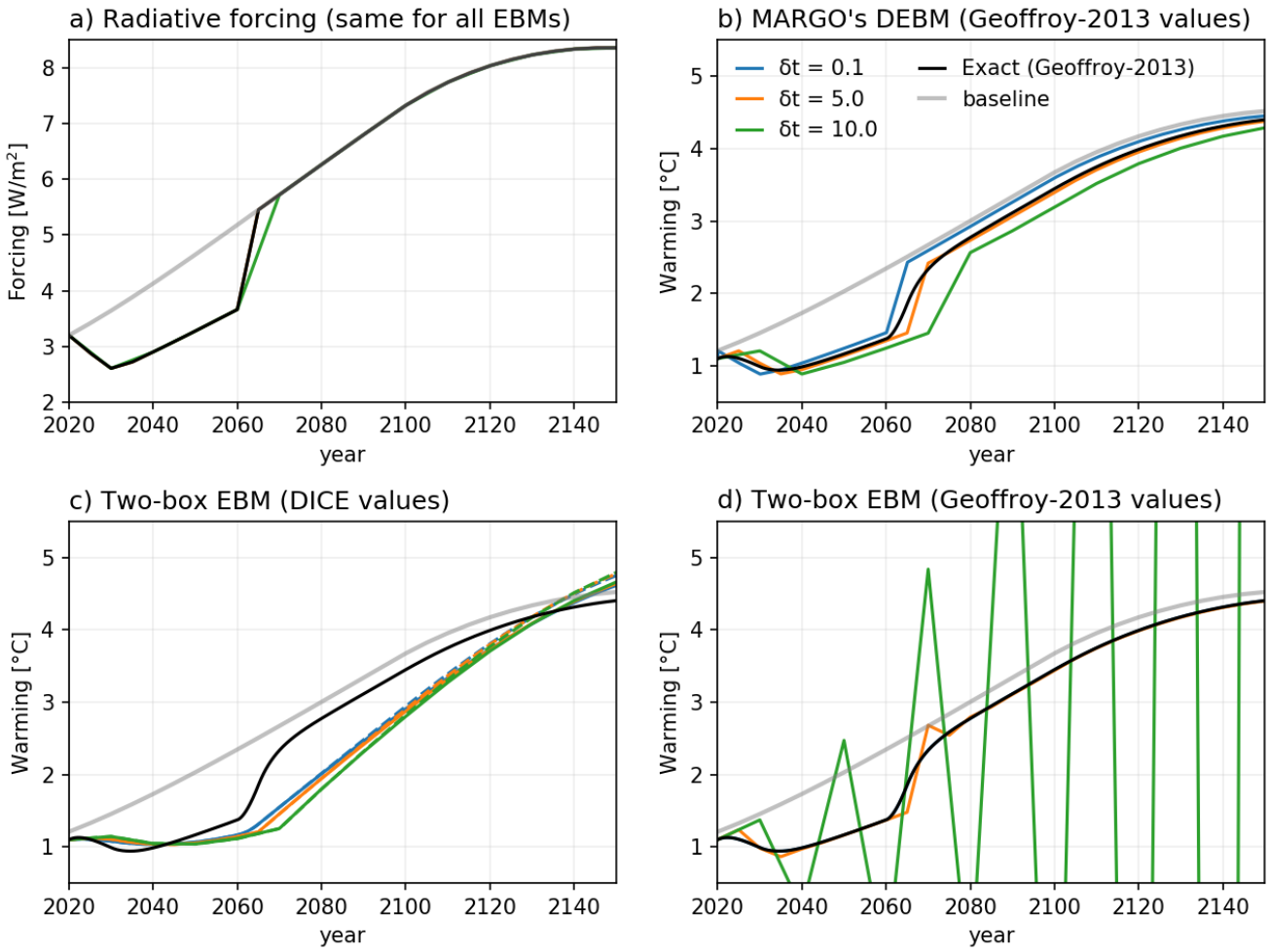

Supplementary Figure S3: (b,c,d) Temperature response of MARGO's Deep-layer Energy Balance Model (DEBM) and several different Energy Balance Model formulations (EBMs) to a forcing scenario (a), corresponding to abrupt deployment and termination of solar radiation modification (SRM) with a background of uncontrolled baseline CO_{2e} emissions. Colored lines show the sensitivity of the different formulations to the discretization timestep δt, with the exact solution of the calibrated EBM from Geoffroy et al. (2012) shown in black.

2020, E_0, and thus $\tilde{\mathcal{C}}_M = 2\%\, E_0/q_0 = \dfrac{2 \text{ trillion USD / year}}{58.5 \text{ GtCO}_2 \text{ / year}} = 0.034 \text{ trillion USD / GtCO}_2 = 34 \text{ USD / tCO}_2$. Since GWP and $q(t)$ increase by similar rates between 2020 and 2100, the instantaneous cost $\mathcal{C}_M(t)$ stays close to 2% during this period.

S2.2 Carbon Dioxide Removal (CDR)

The costs of CDR are set according to bottom-up cost estimates from (Fuss et al., 2018, their Table 2). We compute the mean cost of negative-emissions technologies, where we weight the median cost of each negative-emissions technology (in USD/tCO$_2$) by its upper-bound potential for carbon-dioxide removal (in GtCO$_2$/year). This leads to a total potential of roughly $q_0/2 \approx 26\,\text{GtCO}_2\text{/year}$ at an average cost of $\overline{C}_R = 110\,\text{USD/tCO}_2$. The scaling cost is thus set based on an estimate for $R = 50\%$, i.e. $\mathcal{C}_R \left(\frac{1}{2}\right)^2 = \overline{C}_R\; q_0/2$ or $\mathcal{C}_R = 2\overline{C}_R\; q_0 = 13$ trillion

USD/year.

S2.3 Solar Radiation Modification (SRM)

The costs of SRM largely reflect the costs of unintended climate damages that result due to their imperfect compensation for GHG forcing (Irvine et al., 2017). Relative to both the costs of unintended damages and the costs of other climate controls, the direct costs of SRM measures are thought to be small (McClellan et al., 2012), as in the most commonly studied proposal of releasing gaseous sulfate aerosol precursors into the stratosphere to reflect sunlight back to space. The reference cost of SRM is thus given by $\mathcal{C}_G(t) = \tilde{\mathcal{C}}_G E(t)$, where $\tilde{\mathcal{C}}_G$ is the damage due to deploying $-F_\infty \equiv -F(t \to \infty) = -8.5\,\mathrm{Wm}^{-2}$ worth of SRM, as a fraction of the exogenous GWP $E(t)$. In the face of considerable uncertainties about the climate impacts of large-scale SRM (Irvine et al., 2017), we make the conservative– but arbitrary– assumption that the unintended damages of SRM are as large as the uncontrolled damages due to an equivalent amount of CO_{2e} forcing (as in Belaia et al., 2020; Goes et al., 2011), i.e. $\tilde{\mathcal{C}}_G \equiv \tilde{\beta}(F_\infty/B)^2 \approx 12.6\,\%$, where F_∞/B is the equilibrium temperature response to a fixed radiative forcing of $F_\infty = 8.5\,\mathrm{Wm}^{-2}$.

S2.4 Adaptation

The costs of adaptation are estimated based on a recent joint report commissioned by the United Nations, the Bill and Melinda Gates Foundation, and the World Bank (Global Commission on Adaptation, 2019). They estimate that adaptation measures costing 1.8 trillion USD from 2020 to 2030 generate more than five times as much in total net benefits. However, these net benefits include many co-benefits unattributed to climate change damages and are thus not directly comparable to MARGO's climate change damage function βT^2. Instead, we make the crude assumption that this level of spending reduces climate damages by $A = 10\%$ of the baseline, i.e. $\mathcal{C}_A \left(\frac{1}{10}\right)^2 = 180$ billion USD / year, or $\mathcal{C}_A = 18$ trillion USD / year. Coincidentally, this scaling is similar to that used in the AD-DICE model (de Bruin et al., 2009), although their calibrated cost function has a higher exponent of 3.6 and thus yields smaller costs for low levels of adaptation. By default, we also conservatively cap adaptation at $A < 40\%$, recognizing that adaptation to all climate impacts is impossible: there will always be residual damages that can not be adapted to (Dow et al., 2013). However, this adaptation cap is not reached in any of the simulations presented here, and does not affect the results.

S3 The one-line explicit MARGO formulation

S3.1 Closed-form optimization equations

MARGO's cost-benefit optimization problem is given by

$$\max \{ \text{ discounted net benefits } \},$$

or, in closed form (minus adaptation, for conciseness):

$$\max \Bigg\{ \int_{t_0}^{t_f} (1+\rho)^{-(t-t_0)} \Bigg[q(t)\,\tilde{\mathcal{C}}_M M^2 + E_0(1+\gamma)^{(t-t_0)}\,\tilde{\mathcal{C}_G} G^2 + \mathcal{C}_R R^2 \\ -\beta \Bigg(T_0 + \frac{a \ln\left(\frac{c_0 + \int_{t_0}^{t} r[q(1-M) - q_0 R]\,\mathrm{d}t'}{c_0} \right) - F_\infty G}{B+\kappa} + \frac{\kappa}{B} \int_{t_0}^{t} \frac{e^{\frac{t'-t}{\tau_D}}}{\tau_D} \frac{a \ln\left(\frac{c_0 + \int_{t_0}^{t'} r[q(1-M) - q_0 R]\,\mathrm{d}t''}{c_0} \right) - F_\infty G}{B+\kappa}\,\mathrm{d}t' \Bigg)^2 \Bigg] \mathrm{d}t \Bigg\}, \tag{S7}$$

where $\tau_D = \dfrac{C_D}{B}\dfrac{B+\kappa}{\kappa}$ is a timescale specified by the deep ocean heat capacity parameter C_D.

In MARGO's cost-effectiveness framing, the full optimization problem (minus adaptation, for conciseness) is

$$\min \{ \text{ discounted costs } \} \quad \text{subject to} \quad T_{M,R,G} < T^\star,$$

or, in closed form:

$$\min \left\{ \int_{t_0}^{t_f} \left[q(t)\,\tilde{\mathcal{C}}_M M^2 + E_0(1+\gamma)^{(t-t_0)}\,\tilde{\mathcal{C}_G} G^2 + \mathcal{C}_R R^2 \right] (1+\rho)^{-(t-t_0)}\,\mathrm{d}t \right\}, \tag{S8}$$

subject to

$$T_0 + \frac{a \ln\left(\frac{c_0 + \int_{t_0}^{t} r[q(1-M) - q_0 R]\,\mathrm{d}t'}{c_0} \right) - F_\infty G}{B+\kappa} + \frac{\kappa}{B} \int_{t_0}^{t} \frac{e^{\frac{t'-t}{\tau_D}}}{\tau_D} \frac{a \ln\left(\frac{c_0 + \int_{t_0}^{t'} r[q(1-M) - q_0 R]\,\mathrm{d}t''}{c_0} \right) - F_\infty G}{B+\kappa}\,\mathrm{d}t' < T^\star. \tag{S9}$$

Adaptation is included by adding $\mathcal{C}_A A^2$ to the other control costs in (S8) and subtracting AT from the left hand side of (S9), where T is given by equation (S4).

S3.2 MARGO's intuitive free parameters

A single realization of the MARGO model is fully characterized by the 18 parameters[2] that appear explicitly in equations S8 and S9, the default values of which are reported in Table S1. These 18 parameters are:

- 3 grid parameters t_0, t_f, and δt
- 3 initial conditions T_0, c_0, and $E6_0$;
- 1 carbon cycle parameter r;
- 4 energy balance parameters a, B, κ, and C_D;
- 2 exogenous economic parameters γ and ρ;
- 1 damage cost parameter β
- 4 control cost parameters $\mathcal{C}_A$, $\mathcal{C}_R$, $\tilde{\mathcal{C}}_M$, and $\tilde{\mathcal{C}}_G$.

The 3 grid parameters and 3 initial conditions are dictated by the problem at hand and not typically considered as tuning parameters; thus, in the main text we refer to the other $N = 12$ parameters as MARGO's "free" parameters.

[2]We consider F_∞ a dependent parameter since G can be rescaled such that F_∞ is absorbed into the definition of $\mathcal{C}_G$.

The baseline emissions timeseries $q(t)$ is treated as exogenous and must be prescribed as an input (by default, it is given by a piece-wise linear function described by four additional tunable parameters). In the cost-effectiveness framework, the poorly-constrained damage parameter β is replaced by a prescribed temperature goal $T^\star$. The initial condition and physical parameters are well constrained, while the economic and cost parameters are our heuristic interpretations of the wider climate and economic literature. The grid parameters, on the other hand, are arbitrary user inputs depending on the problem at hand.

We also set maximum deployment and termination rates $\left|\frac{\mathrm{d}\alpha}{\mathrm{d}t}\right| < \dot{\alpha}$, as crude parameterizations of economic, technological, and social inertia (Ha-Duong et al., 1997), which acts to forbid implausibly aggressive deployment (Buck, 2016) and phase-out scenarios. These four parameters enter as additional policy constraints in the optimization, and should also be considered "free" parameters of the MARGO model. We set $\dot{M} \equiv \dot{R} \equiv 1/40\,\mathrm{years}^{-1}$ in line with the most ambitious climate goals (Intergovernmental Panel on Climate Change, 2018) and $\dot{G} = 1/80\,\mathrm{years}^{-1}$ to constrain the initial ramp-up of SRM cooling (except upon SRM termination in Scenario B of Section 4), although this constraint has little impact on the quantitative results. We interpret adaptation deployment costs as buying insurance against future damages at a fixed annual rate $\mathcal{C}_A A^2$, with $\dot{A} = 0$, which can be increased or decreased upon re-evaluation at a later date (see policy response process described in Section 4).

The control variables $\alpha \in \mathcal{A} = \{M, R, G, A\}$ satisfy several additional constraints, which could be thought of as an additional 16 parameters (4 for each of the 4 constraints below), although many are these are either physically necessary or inconsequential in practice because they are turned off in the default configuration or never approached in our optimized scenarios:

1. The controls must be positive, $\alpha \geq 0$;
2. They have an upper bound: $\alpha < \alpha_{\max}$. $M_{\max} = 100\%$ is by set by the definition of mitigation. $G_{\max} = 100\%$ is a normalization choice, which is combined with the definition of F_∞ to result in a negative radiative forcing that exactly offsets the maximum GHG forcing of $F_\infty = 8.5\,\mathrm{W/m^2}$. We set $A_{\max} = 40\%$ in acknowledgement of practical (Dow et al., 2013) and theoretical (Sherwood and Huber, 2010) limits to adaptability (this is meant as more of a symbolic gesture rather than an estimate of how much climate damage might be adaptable). Finally, $R = 100\%$ is set based to roughly twice the value reported by a recent bottom-up assessment of the potential for carbon dioxide removal of existing (but not necessarily scalable) negative emissions technologies.
3. They have an initial condition $\alpha(t_0) = \alpha_0$, which are all set to zero by default, although one could argue that non-zero amounts of mitigation and adaptation have been already deployed at present-day to control some fraction of climate damages.
4. In general, we implement "readiness" constraints, $\alpha(t) = \alpha_{t_0} = 0$ for all $t < t_\alpha$, where t_α is the first year in which the control α is allowed to be deployed. These constraints are included to reflect the fact that some controls, such as geoengineering (both carbon and solar), do not yet exist as climate-relevant socio-technological systems (Flegal et al., 2019). To keep the presentation of the model as simple as possible in the present analysis, we set $t_\alpha = 2020$ for all four controls (no readiness constraints).

Parameter	Default value	Parameter	Default value
a	$4.97\,\mathrm{W/m^2}$	r	50%
B	$1.13\,\mathrm{W/m^2/K}$	κ	$0.72\,\mathrm{W/m^2/K}$
C_D	$106\,\mathrm{W\,yr/m^2/K}$	β	$0.22\,\%\,\mathrm{GWP}\,/\,\mathrm{K^2}$
ρ	2%	γ	2%
$\mathcal{C}_A$	$18 \times 10^{12}\,\mathrm{USD\,yr^{-1}}$	$\mathcal{C}_R$	$13 \times 10^{12}\,\mathrm{USD\,yr^{-1}}$
$\tilde{\mathcal{C}}_M$	$0.034 \times 10^{12}\,\mathrm{USD}\,/\mathrm{GtCO_{2e}}$	$\tilde{\mathcal{C}}_G$	12.6% of GWP / $8.5\,\mathrm{W/m^2}$
t_0	2020	t_f	2200
δt	5 yr	E_0	$100 \times 10^{12}\,\mathrm{USD\,yr^{-1}}$
c_0	460 ppm	T_0	1.1 K

Table S1: Values of the 18 free parameters that characterize the MARGO model, where we distinguish the 12 tuning parameters (top) from the 6 grid and initial condition parameters (bottom).

S4 Optimization method

S4.1 Numerical implementation

We use the Interior Point Optimizer (Wächter and Biegler, 2006) (`https://github.com/coin-or/Ipopt`), an open source software package for large-scale nonlinear optimization, to minimize objective functions representing benefits and costs to society subject to assumed policy constraints (see Section 3.2 and S3.2). In practice, the control variables $\alpha \in \mathcal{A} = \{M, R, G, A\}$ are discretized into $N = (t_f - t_0)/\delta t$ timesteps (by default $\delta t = 5$ years, $N = 36$) resulting in a $4N$-dimensional optimization problem. In the default (deterministic and convex) configuration, and after a one-time 30 second spin-up for just-in-time compiling upon first use, the model takes only $\mathcal{O}(60\,\mathrm{ms})$ to compute optimal solutions and thus effectively provides user feedback in real time (Figure S4a). By comparison, the standard implementation of the DICE-2016r model takes 5 seconds to run, requiring users to wait a non-negligible time to view updated results. This makes the MARGO model amenable to our interactive web applications (see `github.com/ClimateMARGO/ClimateMARGO.jl/gallery.md`), which should be compared to the influential C-ROADS and En-ROADS model web applications (Siegel et al., 2018). Depending on the use case, the timestep can increased to improve performance, although some errors are introduced above the default timestep $\delta t = 5$ years (Figure S4b).

S4.2 Relaxing temperature thresholds in response to overshoots

In the policy response process Scenario A (Section 4.2), we encounter scenarios in which the cost-effectiveness optimization problem has no solutions because climate controls can not longer be deployed rapidly enough to avoid overshooting the warming threshold $T^\star$ (Figure 5). Our solution is to relax the temperature goal upwards as little as necessary until a solution can be found (Figure 5a, transparent solid lines). To do this efficiently, we perform a binary search $T^\star \to T^\star \pm \frac{5\,^\circ\mathrm{C}}{2^n}$ to $n = 12$, i.e. until we sufficiently narrow the range $T^\star_{yes}$ - $T^\star_{no} < 0.001\,^\circ\mathrm{C}$ between

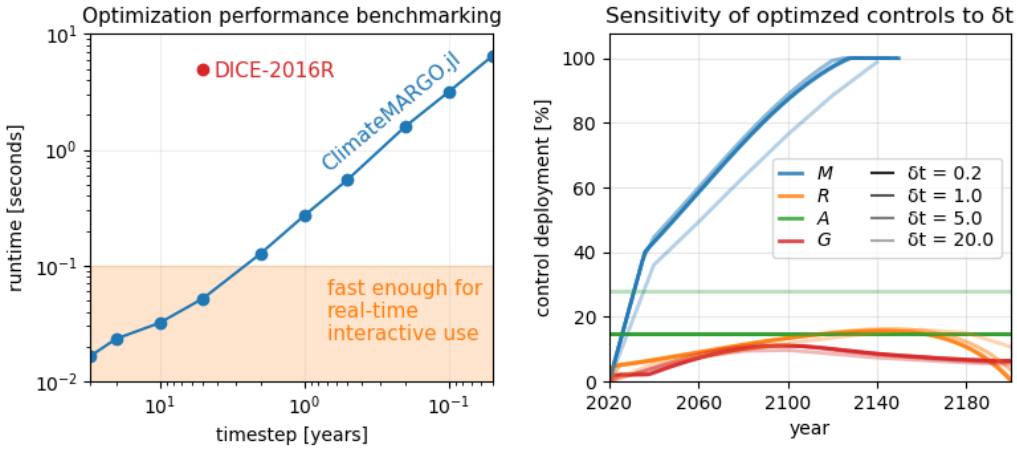

Supplementary Figure S4: Performance benchmarking of MARGO's optimization algorithm. (a) Runtime of ClimateMARGO.jl's optimization function (blue dots) as a function of the model timestep, which is inversely proportional to the dimension of the problem, $N \propto (\delta t)^{-1}$. The self-reported runtime of a single realization of DICE, using its standard GAMS implementation with $\delta t = 5$ years (Nordhaus and Sztorc, 2013), is reported in red. (b) Sensitivity of the accuracy of MARGO's optimized control trajectories (as in Figure 2) to the timestep δt. Results begin exhibiting noticeable errors with $\delta t > 20$ years, but may still be desirable due to increased performance for applications where exact results are not important, such as beta-testing intensive research applications or for interactive educational outreach.

the highest $T^{\star}_{no}$ that admits no solutions and the lowest $T^{\star}_{yes}$ that permits a valid solution.

S4.3 Towards stochastic programming of parametric uncertainties and climate surprises

The model was designed from the beginning with the goal of eventual use in stochastic simulations where 1) the determinstic scalar objective function can be generalized to an expected value (or other statistical metric) of a probabilistic ensemble of simulations that sample an uncertain parameter space and exhibit stochastic dynamics (e.g. stochastic baseline emissions or internal climate variability), and 2) determinstic constraints can be generalized to probablistic constraints (e.g. having a two-thirds chance of keeping temperatures below a goal $T^{\star}$), although these features are still under active development.

Scale analysis based on the high performance of ClimateMARGO's optimization (Figure S4a) suggests that forward uncertainty propagation using Monte Carlo simulations with millions of samples will be possible. Preliminary implementations of a stochastic optimization algorithm using the Sample Average Approximation method also proved promising for low-dimensional problems (< 1000 samples), although it is unclear how these methods will scale for larger problems.

S5 Replicating results of a complementary multi-control optimization model

To illustrate the potential utility of MARGO as a community tool, we show how a few run-time parameter values in MARGO can be tweaked to match the model configurations and results of Belaia et al. (2020), a complementary analysis of optimized multi-control climate policy. Belaia et al. (2020) extend DICE, a commonly-used globally-aggregated general equilibrium IAM, to include carbon dioxide removal (CDR) and solar radiative modification (SRM) to supplement DICE's emissions mitigation in controlling climate damages.

To qualitative replicate the model setup used by Belaia et al. (2020), we make the following changes:

- Extend t_f from 2200 to 2500.
- Modify $q(t)$ to match their multi-centennial baseline emissions curve (Figure S5b). In practice, we found it difficult to reproduce Belaia's forcing curves with CO_{2e} emissions alone, presumably because of the fixed forcing term F_{other} due to other forcing agents which are not mitigated in the DICE formulation (Helwegen et al., 2019). To match their baseline forcing (Figure S5c), we thus tune the baseline emissions by multiplying the CO_2 emissions from Belaia et al. (2020) by 1.2 and increasing the airborne fraction r from 50% to 80%.
- Belaia et al. (2020) assume the marginal cost function for CDR is concave, such that CDR is only deployed at high levels if cheap mitigation has been exhausted first. To qualitatively reproduce this behavior, we decrease the exponent on the CDR cost function from 2 to 1.5, so that CDR costs become $\mathcal{C}_R R^{1.5}$ and marginal CDR costs become $\mathcal{M}_R(R) = \frac{\mathrm{d}(\mathcal{C}_R R^{1.5})}{\mathrm{d}R} = 1.5\,\mathcal{C}_R\sqrt{R}$, and we divide by q_0 to convert to units of USD/tCO_{2e}. We also increase the exponent on mitigation to 2.8 to match DICE. To better match the magnitudes of their marginal cost curves, we multiply our default mitigation cost by 5 and CDR cost by 0.75,; however, our costs do not change over time and are best interpreted as an average cost over the 21st Century, while Belaia et al. (2020)'s costs decrease over time.

Figure S5c shows the results of cost-benefit analysis in this configuration, with the forcing time-series from an analogous run of the Belaia et al. (2020) model overlaid with dashed lines. Without much calibration, MARGO reproduces both the qualitative timing of deployments of the three controls in the Belaia et al. (2020) simulations, as well as their quantitative magnitudes.

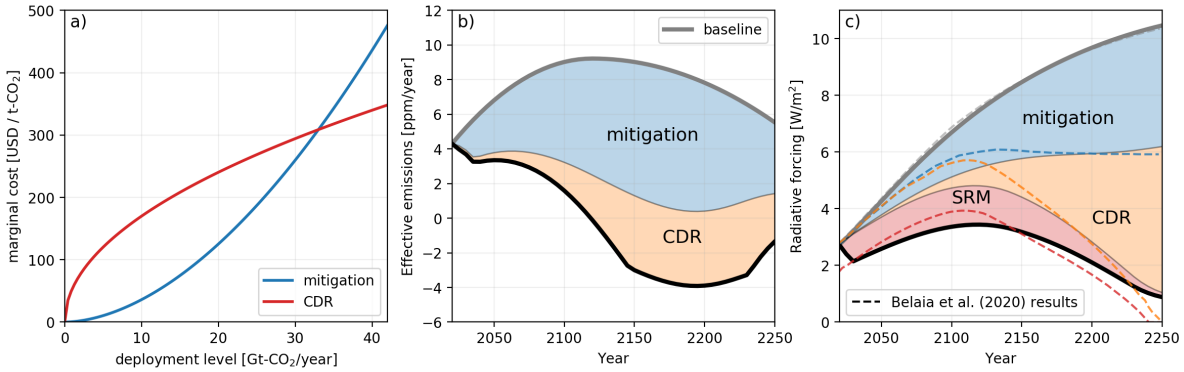

Supplementary Figure S5: A qualitative replication of Figure 4 from Belaia et al. (2020); see their figure caption and accompanying discussion of the results. (a) Marginal cost curves for mitigation and CDR in 2020. (b) Effective emissions. (c) Contributions of mitigation, CDR, and SRM in reducing temperatures, relative to the uncontrolled baseline scenario. Dashed lines show Belaia et al. (2020)'s results while solid lines and shading shows MARGO's replication. Panel (c) is the classic "napkin" diagram, in which SRM is used to shave off a temporary maximum in radiative forcing and is eventually phased out as CDR slowly brings the radiative forcing back down to tolerable levels.

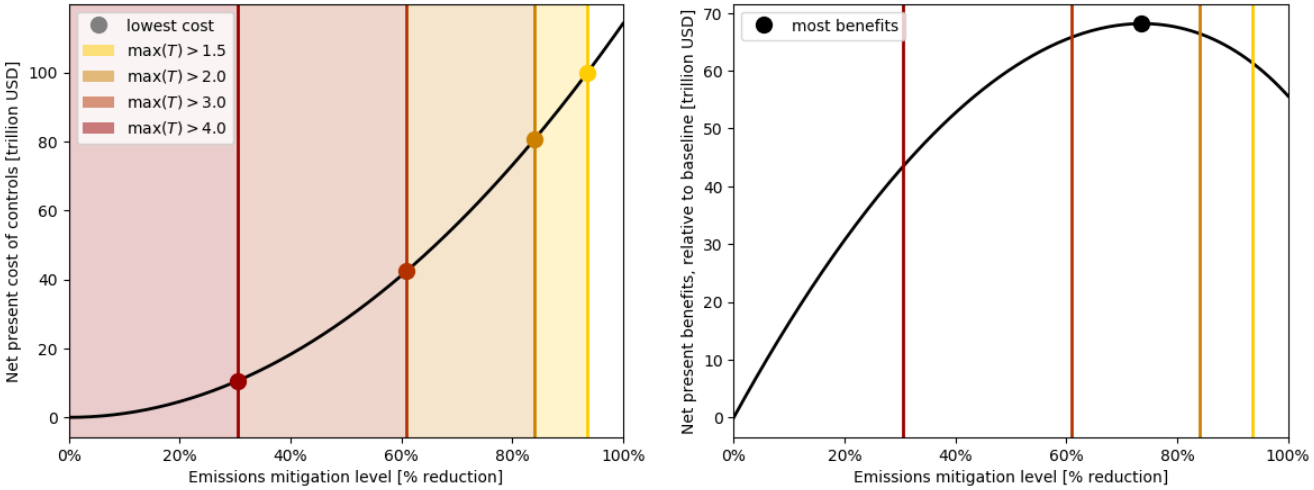

Supplementary Figure S6: A one-dimensional illustration of the cost-effectiveness (left) and cost-benefit (right) optimizations, where we set $R = G = A \equiv 0$ and only control the value of $M \equiv$ constant. (a) The black solid line shows the net present costs of controls (proportional to $\mathcal{C}_M M^2$) as a function of the fractional emissions mitigation M. Shading shows regions with maximum temperatures larger than $T^\star = 4\,^\circ\text{C}, 3\,^\circ\text{C}, 2\,^\circ\text{C}, 1.5\,^\circ\text{C}$, respectively. The colored circles thus denote the most cost-effective (i.e. lowest cost) solutions that satisfy the temperature constraints $T_M < T^\star$. (b) The black curve shows the net present benefits, relative to the no-policy baseline, as a function of the fractional emissions mitigation M. The black circle shows the optimal solution $M = M_{\text{opt}}$ (i.e. most beneficial), which lies at the apex of the benefit curve. Benefits are zero at $M = 0$ by definition, and increase with M until reaching the optimal solution because the benefits of avoided climate damages outweigh the costs of mitigation. For $M > M_{\text{opt}}$, however, the costs of mitigation outweigh the avoided climate damages and thus net benefits begin to decrease with M. The colored vertical lines show maximum temperature contours for context, but they do not directly affect the solution.

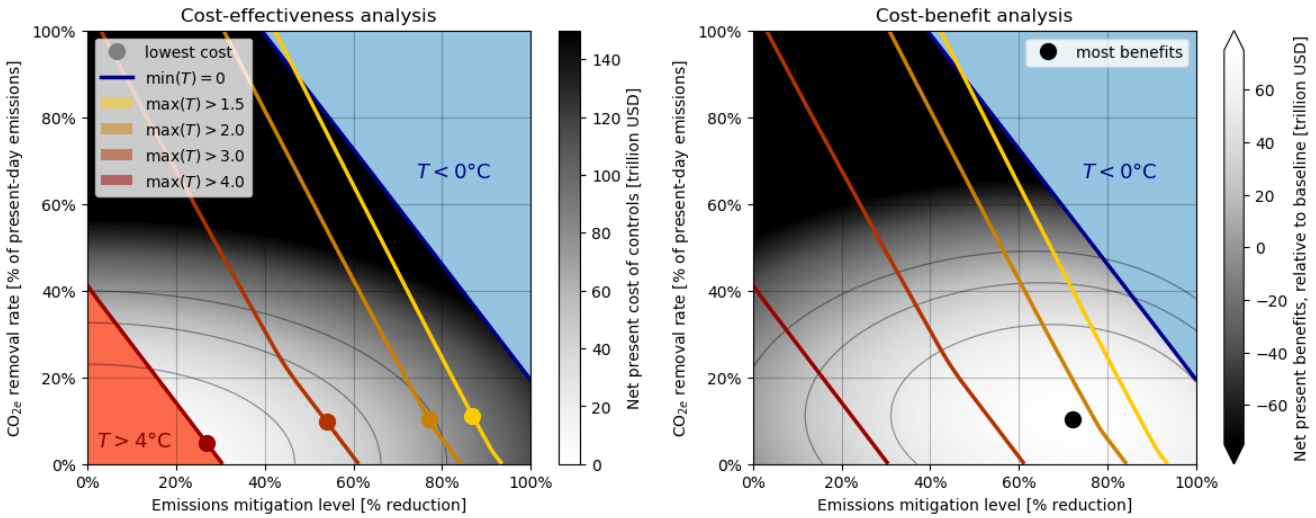

Supplementary Figure S7: Same as Figure S6, but for two-dimensional optimizations, where we set $G = A \equiv 0$ and optimize $M \equiv$ constant and $R \equiv$ constant. Net present control costs and net present benefits are now two-dimensional surfaces (colored, and shown in grey contours), as opposed to curves, and maximum temperature contours are now two-dimensional curves along the cost and benefit surfaces, as opposed to points. Colored circles in the left panel show the most cost-effective solutions, for given threshold temperatures $T^\star$, which are at the minimum of the cost surface along the maximum temperature curve.

References

Belaia, M., Moreno-Cruz, J. B., and Keith, D. W. (2020). Optimal climate policy in three dimensions. Preprint.

Buck, H. J. (2016). Rapid scale-up of negative emissions technologies: social barriers and social implications. *Climatic Change*, 139(2):155–167.

Calel, R. and Stainforth, D. A. (2016). On the Physics of Three Integrated Assessment Models. *Bulletin of the American Meteorological Society*, 98(6):1199–1216. Publisher: American Meteorological Society.

Clarke, L. E., Jiang, K., Akimoto, K., Babiker, M., Blanford, G. J., Fisher-Vanden, K., Hourcade, J.-C., Krey, V., Kriegler, E., Loschel, A., et al. (2014). Assessing Transformation Pathways. In: Climate Change 2014: Mitigation of Climate Change. Contribution of Working Group III to the Fifth Assessment Report of the Intergovernmental Panel on Climate Change. Technical report.

de Bruin, K. C., Dellink, R. B., and Tol, R. S. J. (2009). AD-DICE: an implementation of adaptation in the DICE model. *Climatic Change*, 95(1):63–81.

Dow, K., Berkhout, F., Preston, B. L., Klein, R. J. T., Midgley, G., and Shaw, M. R. (2013). Limits to adaptation. *Nature Climate Change*, 3(4):305–307. Number: 4 Publisher: Nature Publishing Group.

Flegal, J. A., Hubert, A.-M., Morrow, D. R., and Moreno-Cruz, J. B. (2019). Solar Geoengineering: Social Science, Legal, Ethical, and Economic Frameworks. *Annual Review of Environment and Resources*, 44(1):399–423. _eprint: https://doi.org/10.1146/annurev-environ-102017-030032.

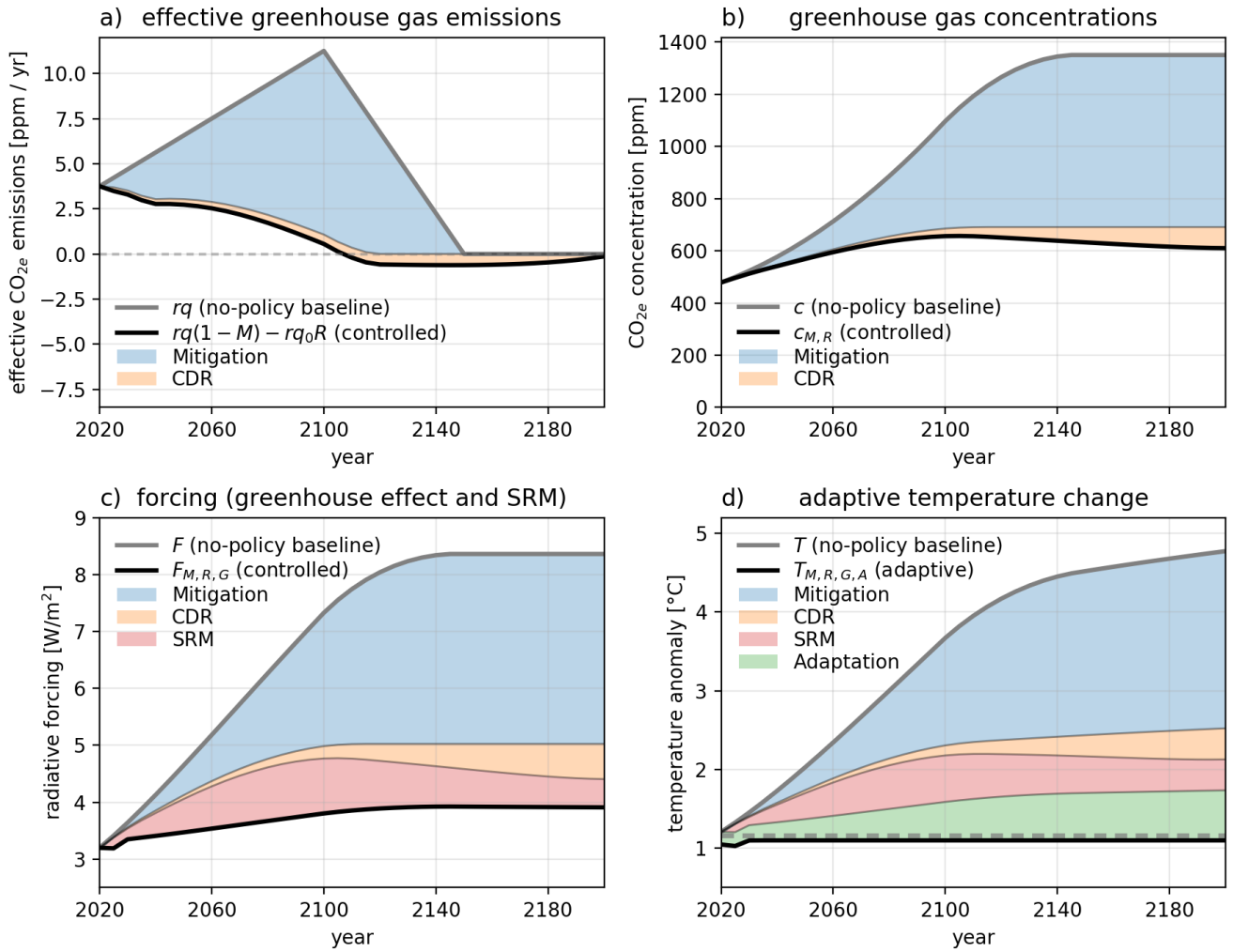

Supplementary Figure S8: Baseline (thick grey lines) and optimally cost-effective (thick black lines) climate outcomes: a) effective CO_{2e} emissions, b) CO_{2e} concentrations, c) radiative forcing, and d) temperature change (relative to preindustrial). Colored wedges show a natural decomposition of the effects of the four different climate controls: **M**itigation (blue); carbon dioxide **R**emoval (CDR; orange); solar radiation modification (SRM) or **G**eoengineering (red); and **A**daptation (green). The dashed grey line in panel d) marks the threshold adaptive temperature of $T^\star = 1.5\,^\circ\mathrm{C}$ to be avoided at all costs.

Fuss, S., Lamb, W. F., Callaghan, M. W., Hilaire, J., Creutzig, F., Amann, T., Beringer, T., Garcia, W. d. O., Hartmann, J., Khanna, T., Luderer, G., Nemet, G. F., Rogelj, J., Smith, P., Vicente, J. L. V., Wilcox, J., Dominguez, M. d. M. Z., and Minx, J. C. (2018). Negative emissions—Part 2: Costs, potentials and side effects. *Environmental Research Letters*, 13(6):063002. Publisher: IOP Publishing.

Geoffroy, O., Saint-Martin, D., Olivié, D. J. L., Voldoire, A., Bellon, G., and Tytéca, S. (2012). Transient Climate Response in a Two-Layer Energy-Balance Model. Part I: Analytical Solution and Parameter Calibration Using CMIP5 AOGCM Experiments. *Journal of Climate*, 26(6):1841–1857. Publisher: American Meteorological Society.

Global Commission on Adaptation (2019). Adapt now: A global call for leadership on climate resilience. Technical

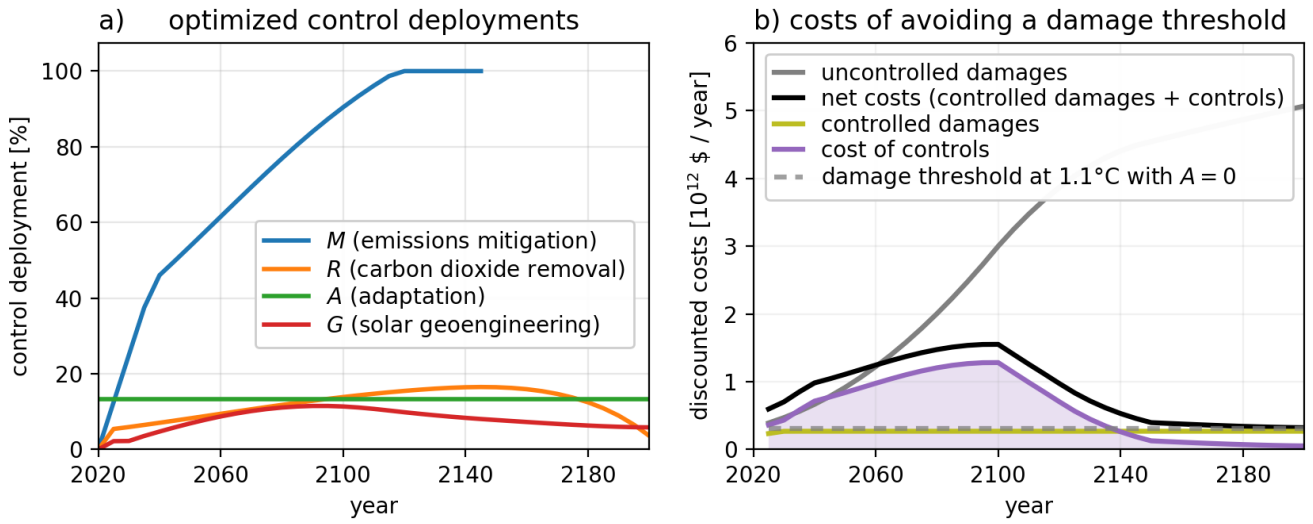

Supplementary Figure S9: Results of cost-effectiveness analysis. (a) Optimized control deployments and (b) corresponding discounted costs and damages. In panel b), the grey line shows the discounted baseline uncontrolled damages; the dashed black line shows the discounted damages associated with 1.1 °C of adaptive pseudo-warming, which are to be avoided at all costs; the orange line shows the discounted damages in the optimally-controlled solution; the red line shows the optimal discounted costs of controls such that the shaded area below is the minimal net present costs of controls (eq. 11), and the black line shows the sum of the control costs (purple) and controlled damages (green). Climate outcomes corresponding to this cost-effectiveness analysis are shown in Figure S8

report.

Goes, M., Tuana, N., and Keller, K. (2011). The economics (or lack thereof) of aerosol geoengineering. *Climatic Change*, 109(3):719–744.

Gregory, J. M. (2000). Vertical heat transports in the ocean and their effect on time-dependent climate change. *Climate Dynamics*, 16(7):501–515.

Gregory, J. M. and Forster, P. M. (2008). Transient climate response estimated from radiative forcing and observed temperature change. *Journal of Geophysical Research: Atmospheres*, 113(D23).

Ha-Duong, M., Grubb, M. J., and Hourcade, J.-C. (1997). Influence of socioeconomic inertia and uncertainty on optimal CO 2 -emission abatement. *Nature*, 390(6657):270–273. Number: 6657 Publisher: Nature Publishing Group.

Hausfather, Z., Drake, H. F., Abbott, T., and Schmidt, G. A. (2020). Evaluating the Performance of Past Climate Model Projections. *Geophysical Research Letters*, 47(1):e2019GL085378. _eprint: https://agupubs.onlinelibrary.wiley.com/doi/pdf/10.1029/2019GL085378.

Held, I. M., Winton, M., Takahashi, K., Delworth, T., Zeng, F., and Vallis, G. K. (2010). Probing the Fast and Slow Components of Global Warming by Returning Abruptly to Preindustrial Forcing. *Journal of Climate*, 23(9):2418–2427.

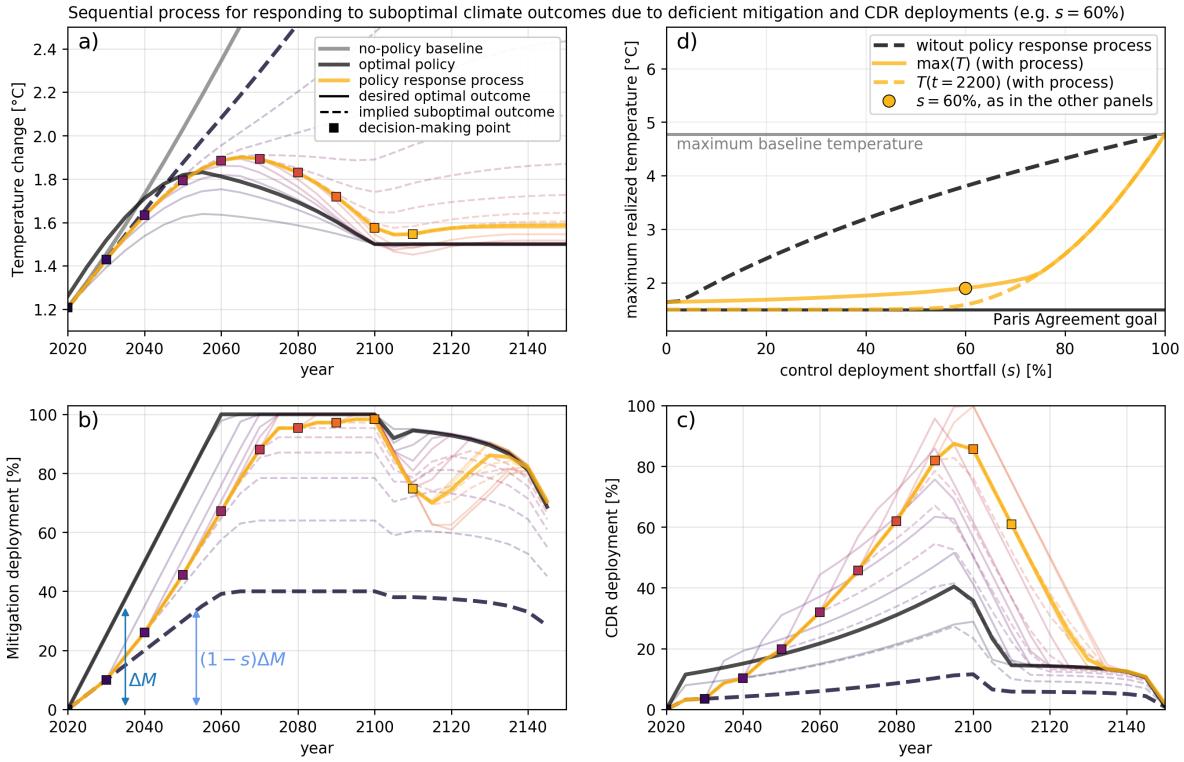

Supplementary Figure S10: **Scenario A (as in Figure 5, but allowing temperature overshoots before 2100):** a globally-aggregated policy decision maker prescribes optimized mitigation and carbon dioxide removal (CDR) trajectories which would limit warming below 1.5 °C by 2100 (thick black lines), but realized deployments repeatedly fall short of these targets by a fraction s, the *short-fall*. In the absence of a policy response, these control shortfalls (thick dashed lines in b, c) lead to a substantial overshoot of the $T^\star = 1.5\,^\circ$C goal (thick dashed line in a). The thick dashed line in Panel b) shows that this overshoot increases roughly linearly with the shortfall s. Panels a)–c) illustrate a policy process for sequentially responding to these control shortfalls every $\Delta t = 10$ years, for $s = 60\%$. After computing an optimized future projection $M \to M + \Delta M$ (thin solid lines), climate controls are incremented sub-optimally $M \to M + (1 - s)\Delta M$ according to the shortfall (dashed lines; see also annotated arrows). After $\Delta t = 10$ years of realized shortfalls (yellow line from one square to the next), the decision maker re-optimizes their prescription of future deployments, and the process repeats. A temporary shortfall in mitigation (c) and CDR (d) results in an overshoot of the temperature goal by 0.4 °C (a), although temperatures are eventually stabilized below $T_{M,R}(2200) = 1.6\,^\circ$C by a delayed decarbonization of $M \approx 100\%$ (c) and intensified CDR deployments (d), which almost entirely offset earlier control shortfalls. Panel b) shows how the maximum realized temperature asymptotes to the temperature goal of 1.5 °C for $s < 30\%$ in the optimal limit and to the catastrophic baseline warming of 4.75 °C in the sup-optimal limit of no climate control ($s \to 100\%$).

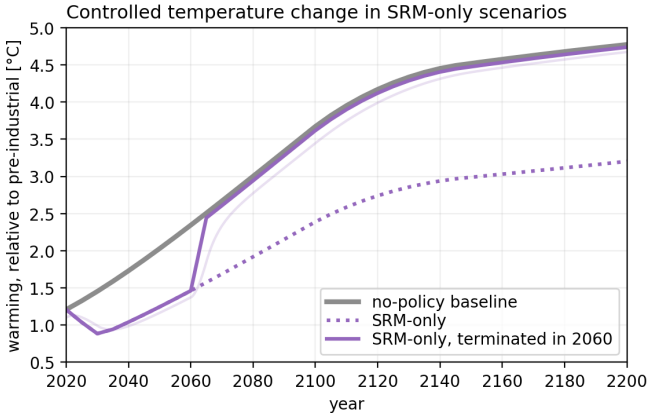

Supplementary Figure S11: **Scenario B:** As in Figure 6, but for the SRM-only scenario, where the lack of mitigation and CDR means that temperatures bounce back up almost to the baseline-warming levels after termination of SRM.

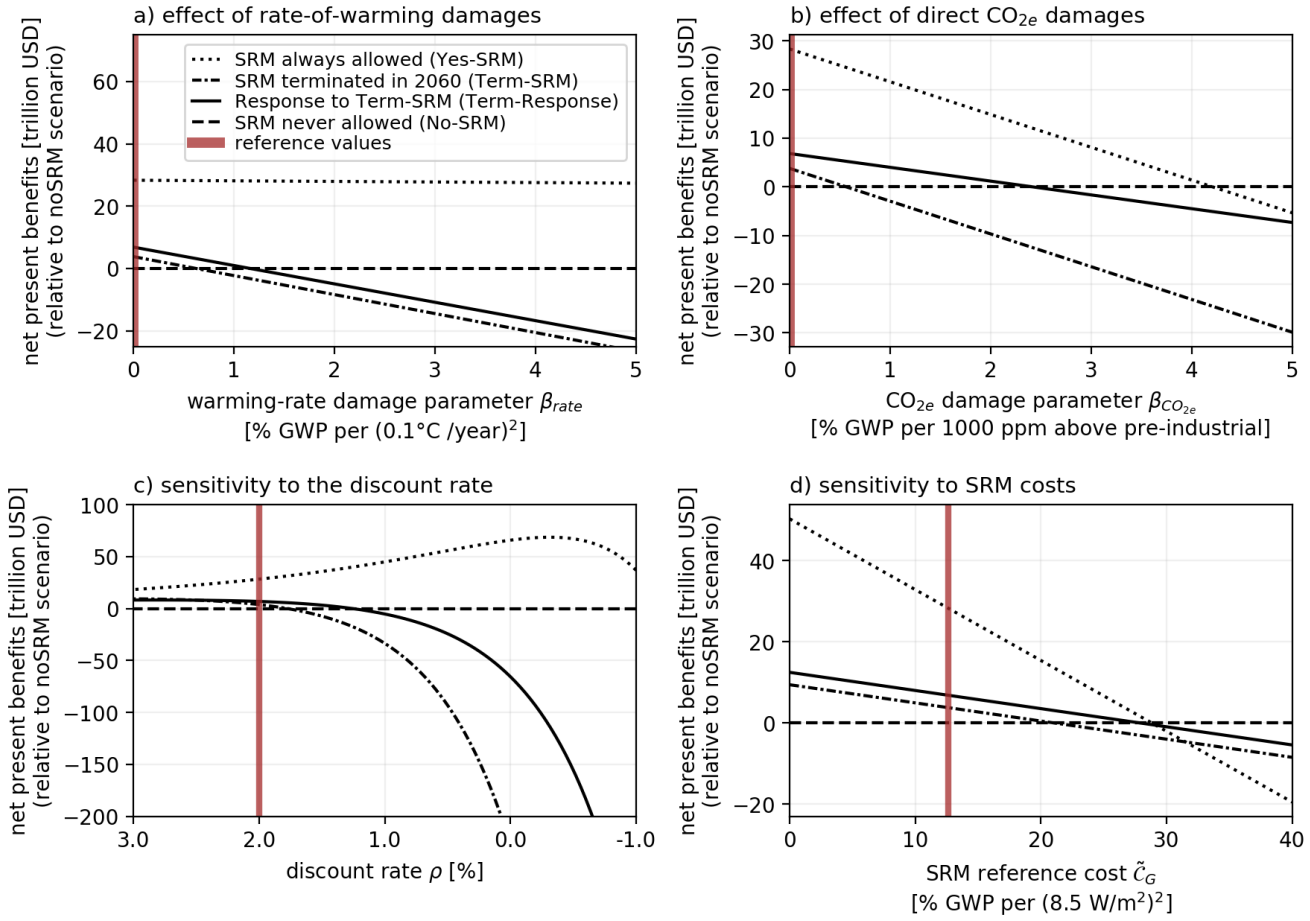

Supplementary Figure S12: Sensitivity of the net present benefits of the Yes-SRM, SRM-Term, Term-Response, and No-SRM trajectories to: an additional damage parameter β_{rate}, where $D_{\text{rate}} = \beta_{\text{rate}} \left(\frac{\partial T}{\partial t}\right)^2$; (b) an additional damage parameter for CO_{2e} concentrations, where $D_{\text{CO}_{2e}} = \beta_{\text{CO}_{2e}} c(t)$; (c) the discount rate ρ; and (d) the SRM damage cost $\mathcal{C}_G$. The additional damage terms are added to the default damage function D when evaluating the net present benefits, but are not active in the optimization that produces these trajectories. Vertical brown lines denote the default values of the parameters.

Helwegen, K. G., Wieners, C. E., Frank, J. E., and Dijkstra, H. A. (2019). Complementing CO_2 emission reduction by solar radiation management might strongly enhance future welfare. *Earth System Dynamics*, 10(3):453–472. Publisher: Copernicus GmbH.

Intergovernmental Panel on Climate Change (2018). *Global warming of 1.5°C*. OCLC: 1056192590.

Irvine, P. J., Kravitz, B., Lawrence, M. G., Gerten, D., Caminade, C., Gosling, S. N., Hendy, E. J., Kassie, B. T., Kissling, W. D., Muri, H., Oschlies, A., and Smith, S. J. (2017). Towards a comprehensive climate impacts assessment of solar geoengineering. *Earth's Future*, 5(1):93–106. _eprint: https://agupubs.onlinelibrary.wiley.com/doi/pdf/10.1002/2016EF000389.

MacMartin, D. G. and Kravitz, B. (2016). Dynamic climate emulators for solar geoengineering. *Atmospheric Chemistry and Physics*, 16(24):15789–15799. Publisher: Copernicus GmbH.

McClellan, J., Keith, D. W., and Apt, J. (2012). Cost analysis of stratospheric albedo modification delivery systems. *Environmental Research Letters*, 7(3):034019. Publisher: IOP Publishing.

Meinshausen, M., Smith, S. J., Calvin, K., Daniel, J. S., Kainuma, M. L. T., Lamarque, J.-F., Matsumoto, K., Montzka, S. A., Raper, S. C. B., Riahi, K., Thomson, A., Velders, G. J. M., and van Vuuren, D. P. (2011). The RCP greenhouse gas concentrations and their extensions from 1765 to 2300. *Climatic Change*, 109(1):213.

Nordhaus, W. and Sztorc, P. (2013). Dice 2013r: Introduction and user's manual. *Yale University and the National Bureau of Economic Research, USA*.

Nordhaus, W. D. (2017). Revisiting the social cost of carbon. *Proceedings of the National Academy of Sciences*, 114(7):1518–1523. Publisher: National Academy of Sciences Section: Social Sciences.

Riahi, K., Grübler, A., and Nakicenovic, N. (2007). Scenarios of long-term socio-economic and environmental development under climate stabilization. *Technological Forecasting and Social Change*, 74(7):887–935.

Sherwood, S. C. and Huber, M. (2010). An adaptability limit to climate change due to heat stress. *Proceedings of the National Academy of Sciences*, 107(21):9552–9555. Publisher: National Academy of Sciences _eprint: https://www.pnas.org/content/107/21/9552.full.pdf.

Siegel, L. S., Homer, J., Fiddaman, T., McCauley, S., Franck, T., Sawin, E., Jones, A. P., Sterman, J., and Interactive, C. (2018). En-roads simulator reference guide. Technical report, Technical Report.

Wächter, A. and Biegler, L. T. (2006). On the implementation of an interior-point filter line-search algorithm for large-scale nonlinear programming. *Mathematical Programming*, 106(1):25–57.